

Wendell P. de Oliveira · Marcelo A. Savi ·
Pedro Manuel C. L. Pacheco

Finite element method applied to the quenching of steel cylinders using a multi-phase constitutive model

Received: 25 June 2012 / Accepted: 16 January 2013 / Published online: 5 February 2013
© Springer-Verlag Berlin Heidelberg 2013

Abstract Heat treatment processes are usually employed to control the mechanical properties of steels and quenching is one of the most common treatments. This article deals with the modeling and simulation of quenching in steel cylinders using a multi-phase constitutive model. Finite element method is employed for spatial discretization. Numerical simulations are carried out by considering an iterative process associated with the operator split technique. Initially, a verification procedure is of concern establishing a comparison between numerical and experimental data, presenting a good agreement. Afterward, notched steel cylinders are treated evaluating the influence of notches in quenched pieces. Temperature, phase transformations and stresses are monitored during the quenching in order to give a general idea of the thermomechanical behavior of the process.

Keywords Quenching · Modeling · Finite element method · Residual stresses · Phase transformations

1 Introduction

Heat treatments are usually employed in industrial processes and quenching is one of the most common treatments. It provides a mean to control mechanical properties of steels as tensile strength, toughness and hardness. The quenching process promotes the formation of different microstructures (ferrite, cementite, pearlite, upper bainite, lower bainite and martensite) that depend on the cooling rate and on the chemical composition of the steel. In general, the combination of phase transformations, large temperature gradients and non-uniform cooling can promote high residual stresses in quenched pieces.

Phenomenological aspects of the quenching involve couplings among different physical processes and their description is unusually complex. Among them, thermal, phase transformation and mechanical processes are important phenomena involved. Several authors have addressed the description of each one of them. Ulysse [56] investigated the thermal response and the residual thermal stresses of forged coated water quench products using numerical and experimental analysis. Sen et al. [46] and Hamouda et al. [14] considered the thermal and residual stress responses of steel pieces without phase transformations. There are also references that focus on

W. P. de Oliveira · M. A. Savi (✉)
Department of Mechanical Engineering, Universidade Federal do Rio de Janeiro, COPPE, 21.941.972, P.O. Box 68.503,
Rio de Janeiro, RJ, Brazil
E-mail: savi@ufrj.br

W. P. de Oliveira
E-mail: wendell@furnas.com.br

P. M. C. L. Pacheco
Department of Mechanical Engineering, CEFET/RJ, 20.271.110, Rio de Janeiro, RJ, Brazil
E-mail: calas@cefet-rj.br

the modeling of the phase transformation phenomenon. In this regard, it is important to understand the existence of diffusive and non-diffusive phase transformations associated with the several micro-constituents involved in quenching process [4–6,17,29,30,37,44]. Sinha et al. [53] and Huiping et al. [20] are other interesting contributions treating multi-phase models.

Quenching is related to high temperature and high loading rates behaviors, and therefore, an elasto-viscoplastic model using a combination of several nonlinear isotropic/kinematic hardening and viscous effects need to be treated in order to obtain a precise description of the thermomechanical behavior of the process. Nevertheless, it is possible to obtain a proper description of the phenomenon with simplified models that consider elasto-plastic behavior with linear kinematic hardening. Several references use this simplified approach presenting good results, where it is important to highlight: [19,24,35,43,57].

Several research efforts considered thermomechanical coupled models that are usually applicable to cylinders [7–12,21–23,32,34,50,51,54,58]. The heat generated during phase transformation can be treated either by considering the latent heat associated with phase transformation or by considering thermomechanical coupling terms in energy equation [9,10,21,36,47,58].

The use of finite element method (FEM) is of special interest in order to allow the analysis of distinct geometries. Silva et al. [48] employed the FEM together with the constitutive model proposed in [47] to study the phase transformation effect in residual stresses generated by quenching in notched steel cylinders. Kang and Im [24–26] presented a modeling effort employing the FEM to perform numerical simulations. Hossain et al. [18] investigated residual stresses in water quenched stainless steel spheres. Lee and Lee [29] and Lee et al. [30] studied geometric distortion in cut cylinders and end-quenched cylinders. Lingamanaik and Chen [33] used a finite element model to assess quenching conditions that promote beneficial compressive residual stresses in the rim of railway wheels.

Based on this scenario, it should be pointed out some previous contributions of the authors' research group. Pacheco et al. [42] discussed the modeling and simulation of quenching, presenting an austenite–martensite model. The proposed model is applied to analyze progressive induction hardening of steel cylinders, showing a good agreement with experimental data. Silva et al. [47] generalized the model including thermomechanical coupling terms, exploiting their importance to the description of quenching process. Afterward, Silva et al. [48] employed the finite element method to evaluate geometric influence on quenching process. Oliveira et al. [37] discussed a constitutive model with diffusional and non-diffusional phase transformations, allowing the description of seven different microstructures, represented by phases in a macroscopic point of view. Quenching of steel cylinders was concerned, showing a good agreement between numerical and experimental tests.

This article deals with the modeling and simulation of quenching in steel cylinders using a multi-phase constitutive model proposed by [37]. The goal here is to employ the finite element method to perform numerical simulations, allowing the analysis of the geometric influence. In this regard, the effect of stress concentrations in phase distributions and residual stresses is of concern, allowing a proper comprehension of the thermomechanical behavior of the quenching process. The proposed numerical procedure is based on the operator split technique associated with an iterative numerical scheme. Under this assumption, the coupled governing equations are solved to obtain the temperature, stress and volume fraction fields from four uncoupled problems: thermal, phase transformation, thermoelastic and elasto-plastic. Classical numerical methods are applied to each one of the uncoupled problems. Numerical simulations are carried out to analyze the quenching of steel cylinders. Initially, a verification procedure is of concern establishing a comparison between numerical simulations and experimental data obtained by the authors in a previous work [37]. Afterward, an investigation of stress concentration is carried out showing the influence of notches in steel cylinders. The use of finite element method together with a general constitutive model is the central contribution of this article.

2 Constitutive model

Constitutive modeling of the quenching process can be performed within the scope of standard generalized materials under the assumption that the thermodynamic state of the material can be completely defined by a finite number of state variables. This approach is based on the thermodynamics stability imposed by the second law of thermodynamics, see e.g., [31]. Under this assumption, the thermomechanical behavior of the material can be described by defining thermodynamical forces obtained from the Helmholtz free energy density, ψ , and thermodynamic fluxes, obtained from the pseudo-potential of dissipation, ϕ [31,37,42].

This approach allows the definition of a complete set of constitutive equations that governs the quenching process. Oliveira et al. [37] assumed an additive decomposition where the total strain ϵ_{ij} is composed by the

following terms: elastic strain, ϵ_{ij}^e ; plastic strain, ϵ_{ij}^p ; thermal expansion strain, ϵ_{ij}^T ; volumetric expansion strain associated with phase transformation, ϵ_{ij}^{tv} ; transformation induced plasticity strain, ϵ_{ij}^{tp} . Therefore, the elastic strain increment can be written as follows:

$$d\epsilon_{ij}^e = d\epsilon_{ij} - d\epsilon_{ij}^p - d\epsilon_{ij}^T - d\epsilon_{ij}^{tv} - d\epsilon_{ij}^{tp} \quad (1)$$

Besides, volume fractions of seven different microstructures, represented by phases in a macroscopic point of view, need to be considered: β_0 (austenite); β_1 (ferrite); β_2 (cementite); β_3 (pearlite); β_4 (upper bainite); β_5 (lower bainite) and β_6 (martensite). Hence, the set of constitutive equations that governs quenching process can be written as follows, defining σ_{ij} as the stress tensor component, X_{ij} as the kinematic hardening tensor and q_i as the heat flux vector:

$$\sigma_{ij} = \sum_{m=0}^6 \beta_m E_{ijkl}^{(m)} \left[\epsilon_{kl} - \epsilon_{kl}^p - \alpha_T^{(m)} (T - T_0) \delta_{kl} - \epsilon_{kl}^{tv} - \epsilon_{kl}^{tp} \right] \quad (2)$$

$$X_{ij} = \left(\sum_{m=0}^6 \beta_m H_{ijkl}^{(m)} \right) \alpha_{kl} \quad (3)$$

$$\dot{\epsilon}_{ij}^p = \lambda \frac{\sigma_{ij}^d - X^d}{\|\sigma_{ij}^d - X^d\|} \quad (4)$$

$$\dot{\alpha}_{ij} = \dot{\epsilon}_{ij}^p \quad (5)$$

$$\dot{\epsilon}_{ij}^{tv} = \sum_{m=1}^6 \gamma^{(m)} \dot{\beta}_m \delta_{ij} \quad (6)$$

$$\dot{\epsilon}_{ij}^{tp} = \sum_{m=1}^6 \frac{3}{2} \kappa^{(m)} f'(\beta_m) \dot{\beta}_m \sigma_{ij}^d \quad (7)$$

$$\dot{\beta}_M = \zeta_{A \rightarrow M} \beta_A^0 [(1 - \beta_M) k \dot{T}] \quad (8)$$

$$\dot{\beta}_m = \zeta_{A \rightarrow m} \left\{ N_m b_m^{\left(\frac{1}{N_m}\right)} (\hat{\beta}_m^{\max} - \beta_m) \left[\ln \left(\frac{\hat{\beta}_m^{\max}}{\hat{\beta}_m^{\max} - \beta_m} \right) \right]^{\left(1 - \frac{1}{N_m}\right)} \right\} \quad (m = 1, \dots, 5) \quad (9)$$

$$q_i = - \left[\sum_{m=0}^6 \beta_m \Lambda^{(m)} \right] T g_i = - \left[\sum_{m=0}^6 \beta_m \Lambda^{(m)} \right] \frac{\partial T}{\partial x_i} \quad (10)$$

In the above equations, the superscript (m) is related to phase m . Under this assumption, each phase has the following properties: $\alpha_T^{(m)}$ is the coefficient of thermal expansion; $\gamma^{(m)}$ is a phase property related to total expansion; $\kappa^{(m)}$ is a material phase parameter. Moreover, δ_{ij} is the Kronecker delta; T and T_0 are, respectively, the temperature and a reference initial temperature; α_{ij} is a variable related to kinematic hardening; \mathcal{E}_{ij}^d is the deviatoric portion of tensor \mathcal{E}_{ij} defined by $\mathcal{E}_{ij}^d = \mathcal{E}_{ij} - \delta_{ij} (\mathcal{E}_{kk}/3)$, and $\|\mathcal{E}_{ij}\|$ denotes the Frobenius norm of tensor \mathcal{E}_{ij} ; $f'(\beta_m)$ expresses the transformation process dependence on the product phase [8, 10, 28]. It should be highlighted that it is assumed two different kinds of phase transformations: non-diffusive and diffusive. Phase transformation from austenite to martensite is a non-diffusive process, which means that the amount of volume fraction is only a function of temperature [5, 6, 44], being described by the Koistinen–Marburger law [27] expressed by Eq. (8). On the other hand, pearlite, cementite, ferrite and bainite formations are diffusion-controlled transformations, which means that they are time dependent. The diffusive transformation kinetics are described by the JMAK law (Johnson–Mehl–Avrami–Kolmogorov) [1, 3], expressed by Eq. (9). The evolution of these phase transformations can be predicted through an approximate solution using data from time–temperature–transformation diagrams (TTT) [5, 37, 44]. In both equations, $\zeta_{A \rightarrow phase(m)}(\dot{T}, t) = \Gamma(-\dot{T}) \Gamma(t_m^f - t) \Gamma(t - t_m^s)$, where $\Gamma(\cdot)$ is the Heaviside function, t_m^s and t_m^f limit the start and finish of the phase transformation. Moreover, N_m , b_m , k , β_A^0 and $\hat{\beta}_m^{\max}$ are parameters related to phase transformations.

Finally, it is important to mention that volume fractions should obey conditions related to phase coexistence and phase transformations represented by the following convex set π :

$$\pi = \left\{ \beta_m \in \Re \mid 0 \leq \beta_m \leq 1 \ (m = 0, 1, \dots, 6); \sum_{m=0}^6 \beta_m = 1 \right\} \quad (11)$$

Concerning plasticity analysis, λ is the plastic multiplier from the classical theory of plasticity where yield surface is defined as follows [31]:

$$v = \left[\frac{3}{2} (\sigma_{ij}^d - X_{ij}^d) (\sigma_{ij}^d - X_{ij}^d) \right]^{1/2} - \left[\sum_{m=0}^6 \beta_m S_Y^{(m)} \right] \leq 0 \quad (12)$$

$S_Y^{(m)}$ is the material yield stress of the m phase and $X_{ij}^d = X_{ij} - \delta_{ij} (X_{kk}/3)$.

The first law of thermodynamics establishes that the energy balance can be written as follows [41]:

$$\frac{\partial}{\partial x_i} \left(\left[\sum_{m=0}^6 \beta_r \Lambda^{(m)} \right] \frac{\partial T}{\partial x_i} \right) - \rho \left[\sum_{m=0}^6 \beta_m c^{(m)} \right] \dot{T} = - \sum_{m=1}^6 \Delta H^{(m)} \dot{\beta}_m \quad (13)$$

where the right term represents thermomechanical coupling terms being represented as a latent heat release during phase transformations [9, 12, 58]; $\Delta H^{(m)}$ is the enthalpy variation in a transformation process involving austenite, the original phase, and product phase β_m ($m = 1, \dots, 6$). Therefore, this source term is used instead of all thermomechanical coupling terms, representing a first approach of the general formulation [47].

A detailed description of the model can be found in [38, 42, 47, 48] and [37].

2.1 Numerical procedure

This contribution considers cylindrical bodies as an application of the proposed general formulation. An axisymmetric finite element model is developed to study through hardening and progressive induction hardening processes in cylinders. Therefore, only radial, r , circumferential, θ , and longitudinal, z , components need to be considered. For this case, tensor quantities presented in the previous section may be replaced by scalar or vector quantities. As examples, one could mention: $\sum_{m=0}^6 \beta_m E_{ijkl}^{(m)}$ replaced by $\sum_{m=0}^6 \beta_m E^{(m)}$; $\sum_{m=0}^6 \beta_m H_{ijkl}^{(m)}$ replaced by $\sum_{m=0}^6 \beta_m H^{(m)}$; σ_{ij} replaced by σ_i ($\sigma_r, \sigma_\theta, \sigma_z$). A detailed description of these simplifications can be found in [42, 47–49] and [39].

The numerical procedure here proposed is based on the operator split technique [40, 41, 52] associated with an iterative numerical scheme in order to deal with nonlinearities in the formulation. Under this assumption, coupled governing equations are solved from four uncoupled problems: thermal, phase transformation, thermoelastic and elasto-plastic. A brief description of each one of them is now presented.

Thermal problem—Comprises a conduction problem with convection and radiation. Material properties depend on temperature and, therefore, the problem is governed by nonlinear parabolic equations. Finite element method is used for numerical solution to obtain the temperature field induced by the thermal boundary conditions and the latent heat associated with phase transformation.

Phase transformation problem—The volume fractions of the phases are determined by integrating evolution equations employing the implicit Euler method considering the temperature field obtained in the previous step associated with the thermal problem.

Thermoelastic problem—Stress and displacement fields are evaluated from temperature distribution. Numerical solution is obtained employing the finite element method.

Elasto-plastic problem—Stress and strain fields are determined considering the plastic strain evolution in the process. Numerical solution is based on the classical return mapping algorithm [52].

Figure 1 presents an overview of the numerical scheme: y represents a vector containing the model internal variables, i is the iteration step and Tol is a prescribed numerical tolerance associated with the convergence of the iterative process.

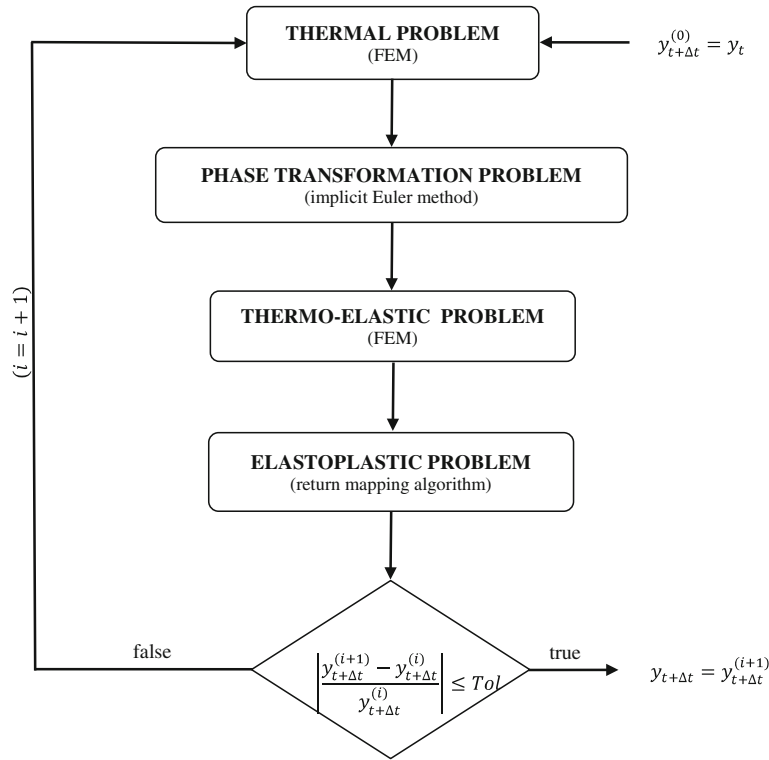


Fig. 1 Iterative numerical scheme based on the operator split technique

3 Analysis of a steel cylinder

The forthcoming analysis promotes a verification of the proposed model establishing a comparison with experiment data obtained in [37]. The main goal here is to validate finite element procedure based on experimental results. The experimental procedure is a through hardening of cylindrical specimens heated to a temperature above the critical value (830 °C), holding at that temperature for 1 h to promote the complete austenitizing of the workpiece. Afterward, a cooling process is performed considering two different media: air and water. Thermocouples (type K), housed in a 1.5-mm-diameter inconel cover, are introduced at each hole in order to monitor the temperature time history that is registered by a data acquisition system. An uncertainty of approximately 5 °C is expected. After the quenching process, metallographic samples are prepared by the conventional technique of manual grinding and polishing followed by chemical etching with nital 2 % reagent. The characterization of the resulting microstructure is carried out by optical microscopy and the volume fraction of phases is determined by the point count technique. In the present work, a grid of 100 points is applied over 10 fields over the sample, which results in 1,000 points and an uncertainty less than 5 % is expected. Besides model verification, this section also presents an analysis of stress evolution during the process.

An SAE 4140H cylinder specimen with 25.4 mm (1") radius is considered with the following chemical composition (wt%): C 0.38 %; Mn 0.64 %; Cr 0.99 %; Mo 0.16 % is adopted [45]. Quenching process is performed in two different cooling media: air and water.

Material parameters of the SAE 4140H are the following [8,10,34,39,54,58]: $\gamma_1 = 3.333 \times 10^{-3}$, $\gamma_2 = 0$, $\gamma_3 = \gamma_4 = \gamma_5 = 5.000 \times 10^{-3}$, $\gamma_6 = 1.110 \times 10^{-2}$, $\kappa^{(m)} = [5/(2S_Y^0)]\gamma^{(m)}$ (where S_Y^0 is the austenite yielding stress and $m = 1, \dots, 6$); $\rho = 7.800 \times 10^3 \text{ kg/m}^3$, $M_s = 340 \text{ }^\circ\text{C}$, $M_f = 140 \text{ }^\circ\text{C}$. Other parameters depend on temperature and need to be interpolated from experimental data. Therefore, parameters $E^{(m)}$, $H^{(m)}$, $S_Y^{(m)}$, $\alpha_T^{(m)}$, $c^{(m)}$, $\Lambda^{(m)}$ ($m = 1, \dots, 6$) and the convection coefficient, h , are evaluated by polynomial expressions [13,15,16,34,37,42,47]. Temperature dependent parameters for diffusive phase transformations are obtained from TTT diagrams [2]. Moreover, latent heat release associated with the enthalpy variations in transformation process involving a parent phase (austenite) and a product phase β_m is given by: $\Delta H^{(3)} = \Delta H^{(4)} = \Delta H^{(5)} = 1.56 \times 10^9 - 1.5 \times 10^6 T \text{ J/m}^3$, $\Delta H^{(6)} = 640 \times 10^6 \text{ J/m}^3$ [9,55,58].

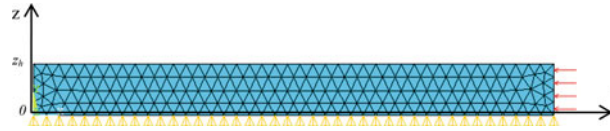


Fig. 2 Finite element mesh and boundary conditions

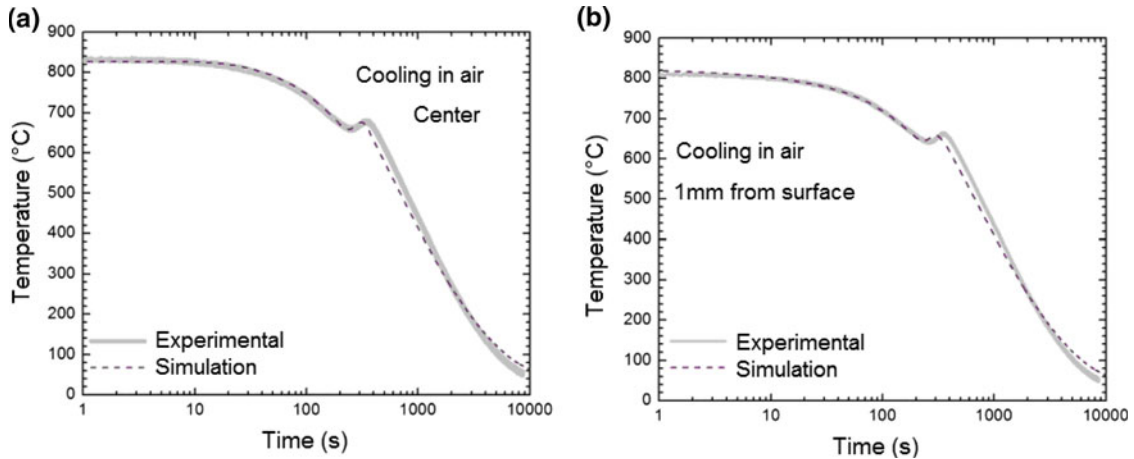


Fig. 3 Air cooling temperature time history: **a** at the center and **b** at 1 mm from the cylinder surface

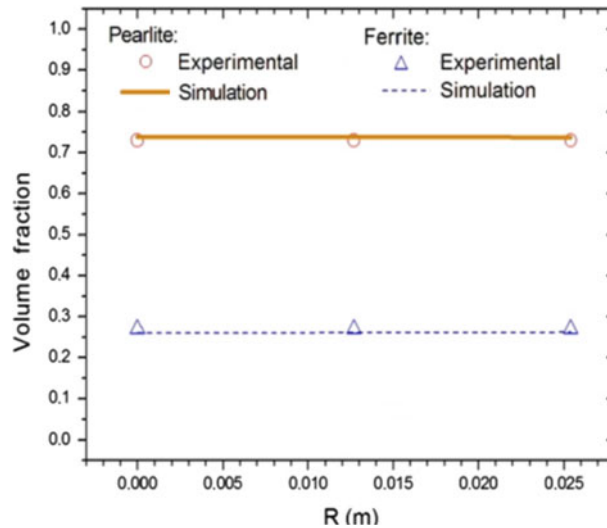


Fig. 4 Phase distribution along the cylinder radius

Finite element analysis is performed exploiting a single-strip axisymmetrical geometry. This assumption can be employed to treat long cylinders subjected to quenching, far from the ends, since the process along the cylinder is similar. Figure 2 shows the axisymmetric finite element model mesh obtained after a convergence analysis, where z is the axisymmetry axis. The following mechanical and thermal boundary conditions are adopted: prescribed z -direction null displacement at $z = 0$ (symmetry condition); prescribed z -direction null heat flux at $z = 0$ and $z = z_h$; convection and radiation on external surface (red arrows).

3.1 Model verification

Initially, model verification is of concern treating air cooling quenching. Experimental data obtained by [37] are used as a reference in order to compare numerical and experimental results. Figure 3 presents the temperature

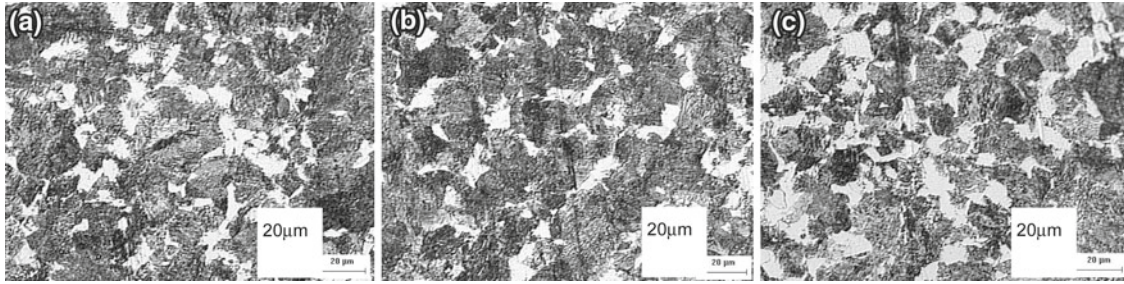


Fig. 5 Air cooling specimen microstructure (etching nital 2%): **a** center ($r = 0$), **b** $r = 0.50R$ and **c** surface ($r = R$)

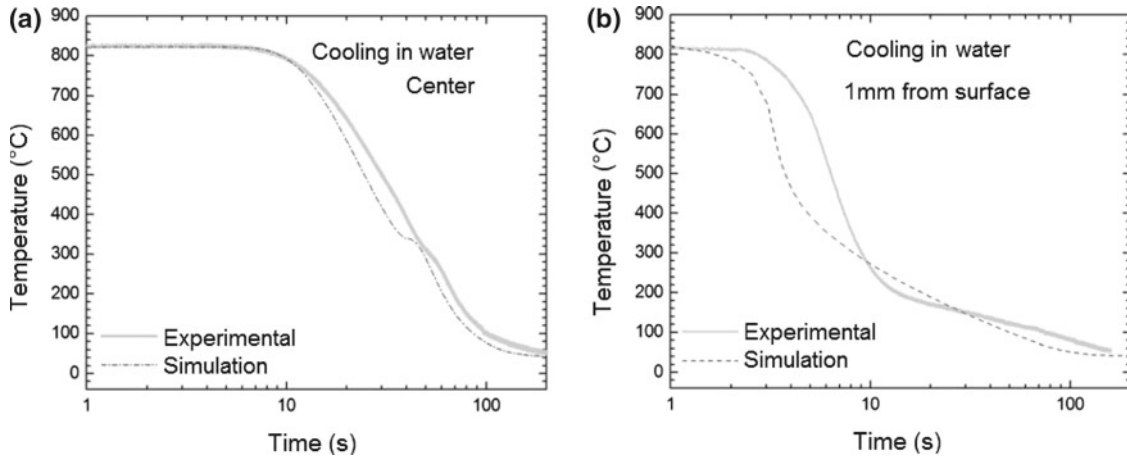


Fig. 6 Air cooling temperature time history: **a** at the center and **b** at 1 mm from the surface for the cylinders

time history in two different positions: at the center and at 1 mm from the surface of the cylinder. The close agreement between the results is noticeable. It is important to highlight that the thermomechanical coupling effect is captured by the model, showing the temperature increase around 650 °C, which is associated with the latent heat of the austenite → pearlite phase transformation. In terms of volume fraction distribution, model predicts 27 % of ferrite and 73 % of pearlite. Once again, this is in close agreement with experimental results, as presented in Fig. 4. The microstructure at internal cross-sections of the cylinder far from the edges, at three regions ($r = 0$, $r = 0.5R$ and $r = R$), is presented in Fig. 5. The metallographic analysis reveals a homogeneous radial phase distribution with 24 % of ferrite and 76 % of pearlite.

The quenching process is now performed using water as a cooling medium. Once again, experimental data obtained by [37] are used as a reference. Temperature time histories in two different positions (at the center of the cylinder and at 1 mm from the cylinder surface) are presented in Fig. 6. At the center of the body, there is a close agreement between numerical and experimental results. By considering the position at 1 mm from the surface, on the other hand, results capture just the general behavior. This discrepancy is explained by the thermocouple influence. Oliveira et al. [37] discussed adjustments that include the heat conduction through the thermocouple that should be considered in order to evaluate the temperature at the cylinder center. In terms of volume fraction distribution, the model predicts 100 % of martensite at the surface and 91 % at the center of the cylinder. This implies an amount of 9 % of bainite that is a small difference when compared to experimental data. Figure 7 shows the phase distribution along the cylinder radius while Fig. 8 presents micrograph results related to this test.

3.2 Stress analysis

Numerical simulations of the behavior of the stress field during the quenching process with air cooling is now in focus. Figure 9 presents the evolution of the normal stresses (σ_r , σ_θ and σ_z) during the process for five different positions: $r = 0$; $r = 1/4R$; $r = 1/2R$; $r = 3/4R$; $r = R$. Figure 9a, b have two panels where the lower one is just an amplification of the upper one. Component $\tau_{r,z}$ has low values during all the process, and therefore, is

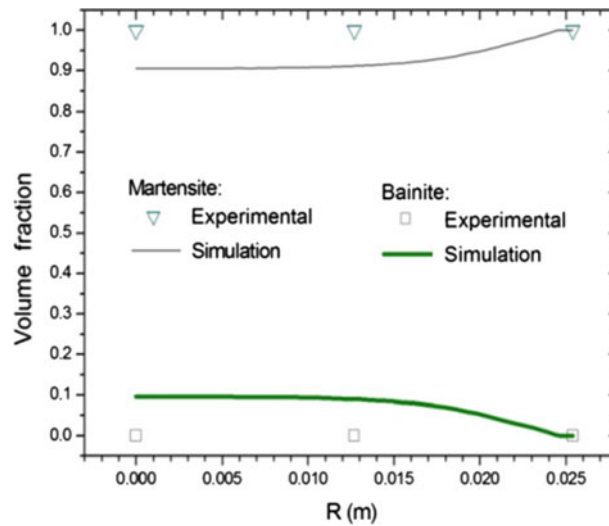


Fig. 7 Phase distribution along the cylinder radius

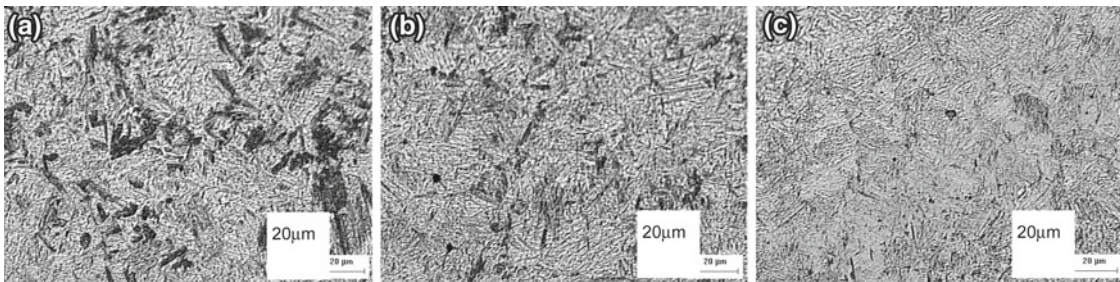


Fig. 8 Water cooling specimen microstructure (Etching nital 2%): **a** center ($r = 0$), **b** $r = 0.50R$ and **c** surface ($r = R$)

neglected in the analysis. Basically, the stress evolution can be understood by analyzing the main phenomena observed during the process. Therefore, it is possible to identify three stages: high temperature behavior—where the cooling process is starting and phase transformations do not take place; phase transformation stage and low temperature behavior—representing the end of the cooling where phase transformations are finished.

Initially, the cylinder is at high temperature where austenite is the stable phase. Before the cooling starts, normal stresses have values close to zero in the whole piece. During this stage, stress components tend to increase values, reaching a plateau. Component σ_z tends to vanish in the whole piece during all this stage. The σ_r stress component is always null at the cylinder surface ($r = R$) due to mechanical boundary conditions. Convection and radiation phenomena induce faster cooling at the cylinder surface promoting a contraction of this region in contrast of the expansion at the center of the cylinder. In general, it is possible to observe that σ_r presents compressive behavior at the center of the cylinder, tending to vanish near the surface; σ_θ presents tensile values at the cylinder surface and compressive at the center.

The phase transformation stage has an important influence in the stress distribution during the quenching. During this stage, two different phenomena establish a competition to define the thermomechanical behavior of the material: phase transformation and thermal effects. This competition promotes a complex behavior of stress components during this stage. Initially, phase transformation effects are preponderant and, at the end of this stage, thermal effects become more relevant. Basically, phase transformations are related to the transformation from austenite to pearlite and ferrite. Austenite–pearlite transformation generates high values of stress levels when compared to those related to austenite–ferrite phase transformation. The component σ_z tends to vanish during all the stage; σ_r presents compressive values at the beginning and at the end of this stage, for the whole piece. Component σ_θ presents compressive behavior at the center and tensile behavior at the surface during the beginning and the end of this stage, presenting a complex behavior between these instants. Moreover, it is important to observe that σ_θ presents critical behavior due to higher values compared with other components

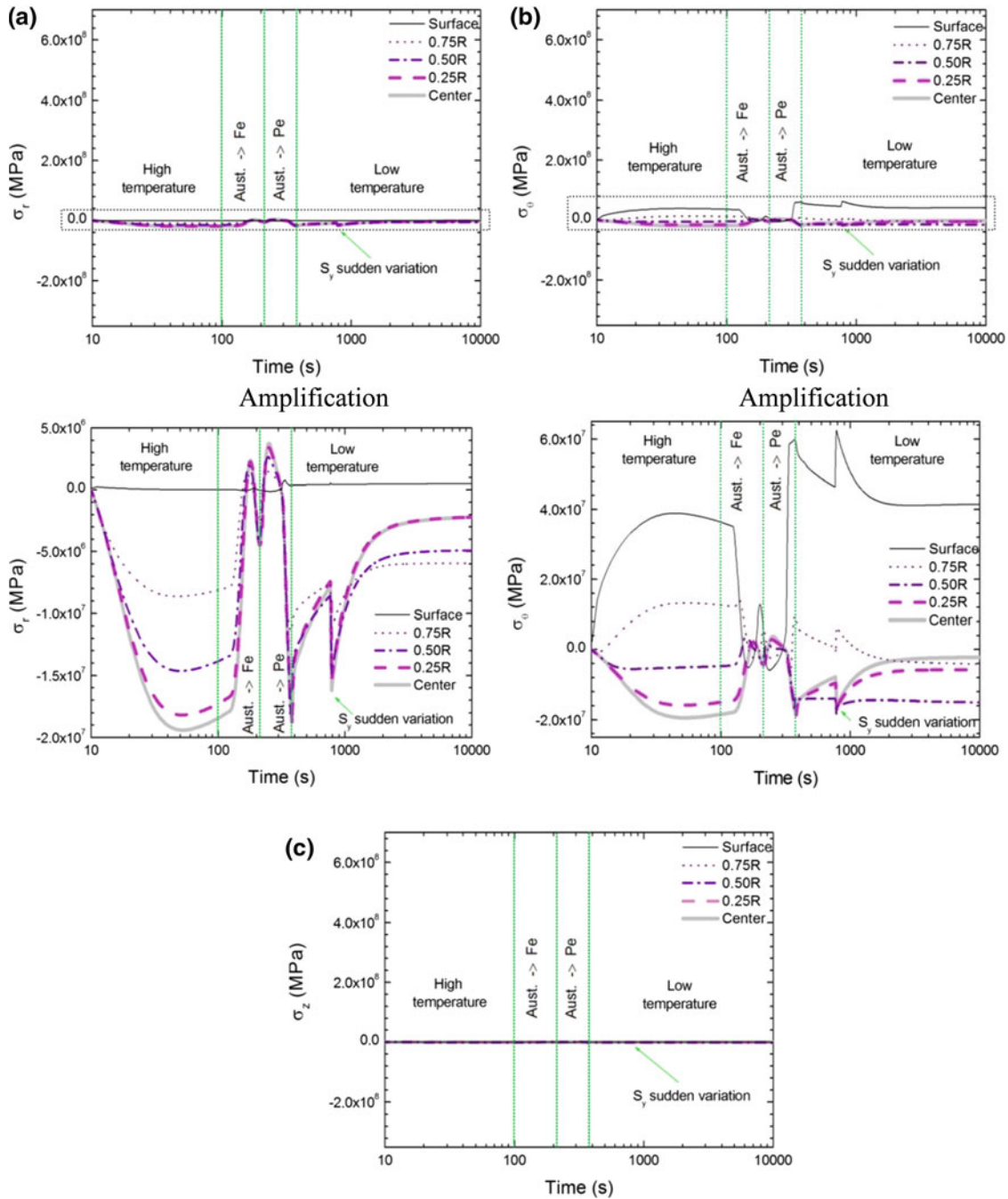


Fig. 9 Stress distribution during the time: **a** σ_r , **b** σ_θ and **c** σ_z

and also due to tensile behavior at the surface. It is important to point that part of the residual stresses is absorbed by transformation plasticity.

After the phase transformation stage, temperatures at the cylinder surface are smaller than the temperatures at the center of the specimen. For temperatures above 475 °C, the yield stress has low values, and therefore, part of residual stresses is vanished. The normal stress behavior presents the same qualitative behavior of the high temperature behavior.

The stress analysis of quenching using water as a cooling medium is now in focus. Figure 10 presents the evolution of normal stresses (σ_r , σ_θ and σ_z) for five different positions: $r = 0$; $r = 1/4R$; $r = 1/2R$; $r =$

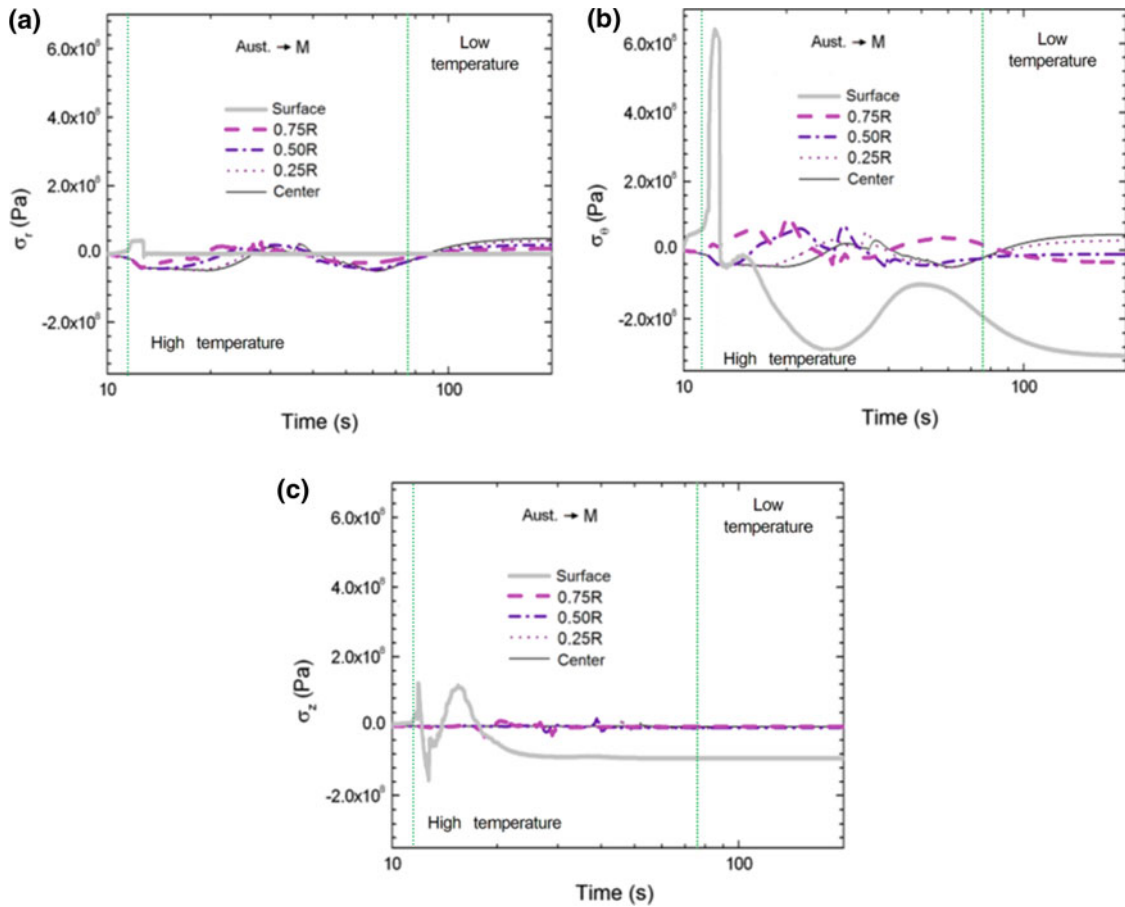


Fig. 10 Stress distribution during the time: **a** σ_r , **b** σ_θ and **c** σ_z

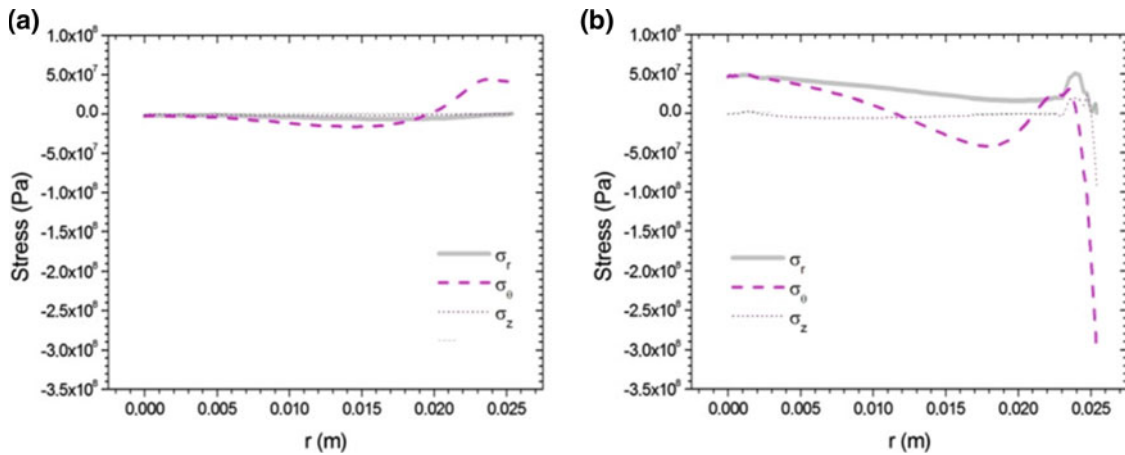


Fig. 11 Stress distribution at the end of the process: **a** air and **b** water cooling

$3/4R$; $r = R$. Once again, it is possible to identify three stages during quenching: high temperature behavior, phase transformation and low temperature behavior.

Before the cooling starts, normal stresses have values close to zero in the whole piece. During this stage, stress components tend to increase values, reaching a plateau. Component σ_z tends to vanish in the whole piece during all this stage. The σ_r stress component is always null at the cylinder surface ($r = R$) due to mechanical

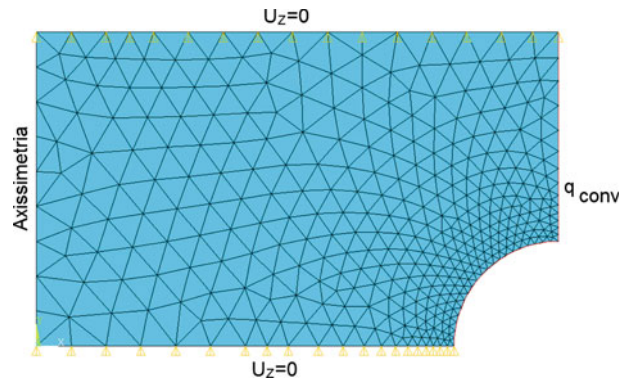


Fig. 12 Boundary conditions: geometries with stress concentrators

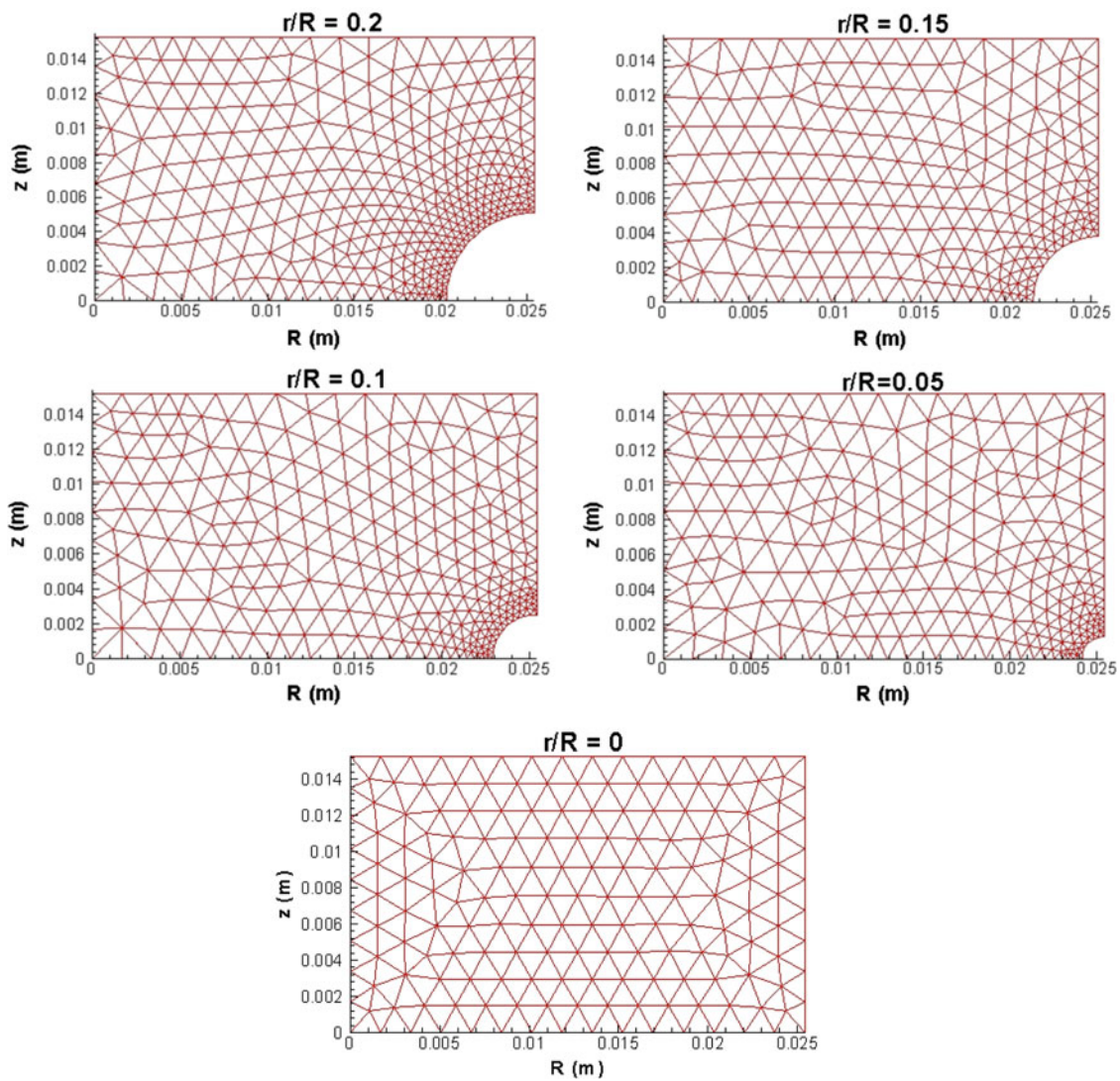


Fig. 13 Notched cylinders and meshes adopted in simulations

boundary conditions. Convection phenomenon induces faster cooling at the cylinder surface promoting a contraction of this region in contrast of the expansion at the center of the cylinder. In general, it is possible to observe that σ_r presents compressive behavior at the center of the cylinder, tending to vanish near the surface;

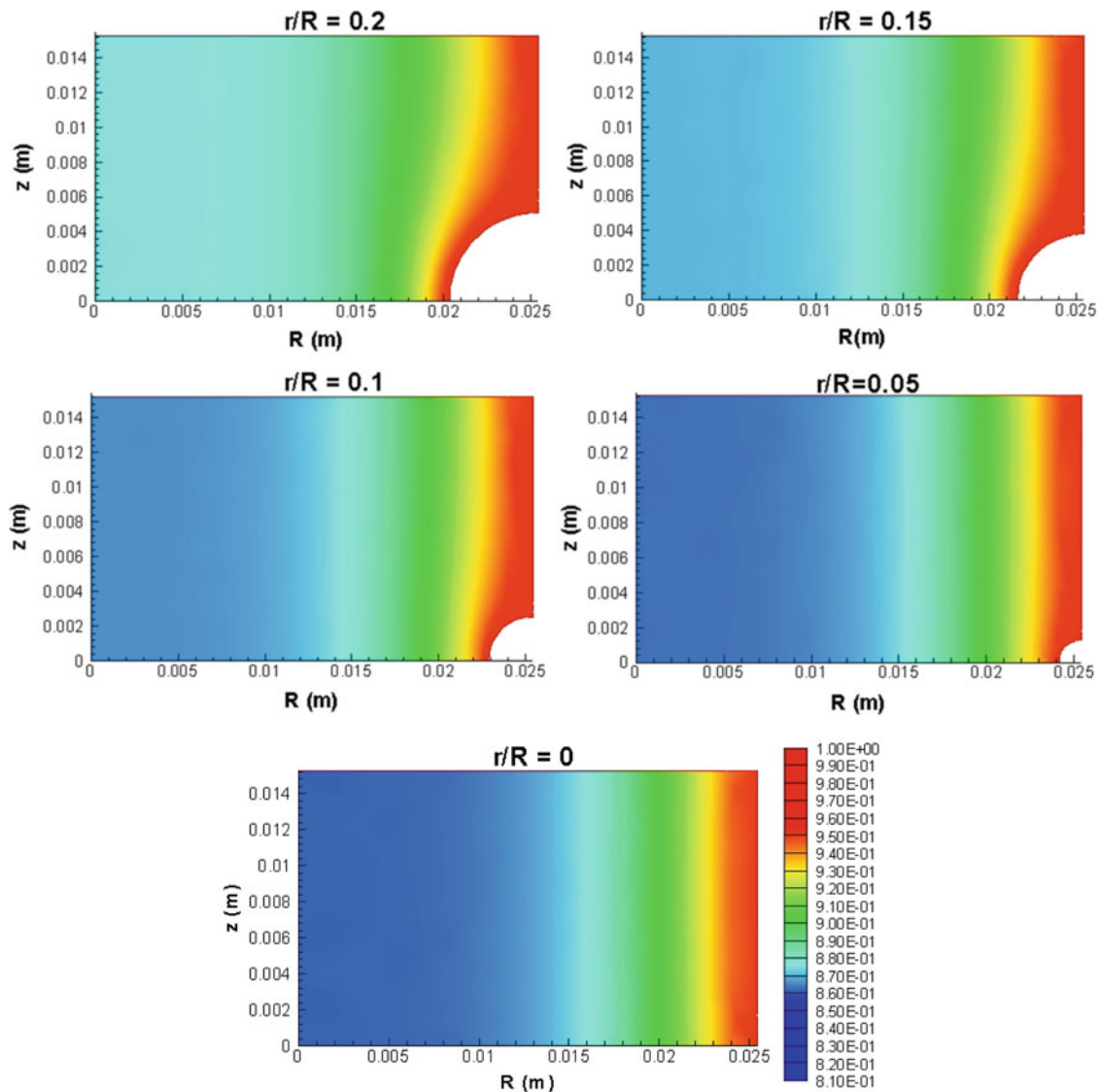


Fig. 14 Martensite volume fraction distribution for different geometries

σ_θ presents tensile values at the cylinder surface and compressive at the center; σ_z presents values that tend to vanish in almost the whole piece.

The phase transformation stage in this quenching process has the characteristic that martensitic phase transformation is the most important phenomenon. Nevertheless, there are also transformations from austenite to upper bainite and lower bainite. Phase transformation establishes a competition with thermal effects to define the thermomechanical behavior of the material. Initially, phase transformation effects are preponderant with volumetric expansion as an important phenomenon; at the end of this stage, thermal effects become more relevant, and high temperature gradients are essential. The component σ_z tends to vanish during all the stage, except to surface; σ_r values increases at the beginning of this stage, being tensile at the center of the cylinder and zero at the surface, after that, these values decreases, being compressive at the center of the cylinder and zero at the surface. Component σ_θ increases at the beginning of this stage, after a short period of time, this stress decreases, becoming compressive in almost the whole piece.

After the phase transformation stage, temperatures at the cylinder surface are still smaller than the temperatures at the center of the specimen. These temperatures reach an equilibrium condition after a period of time (around 200 s).

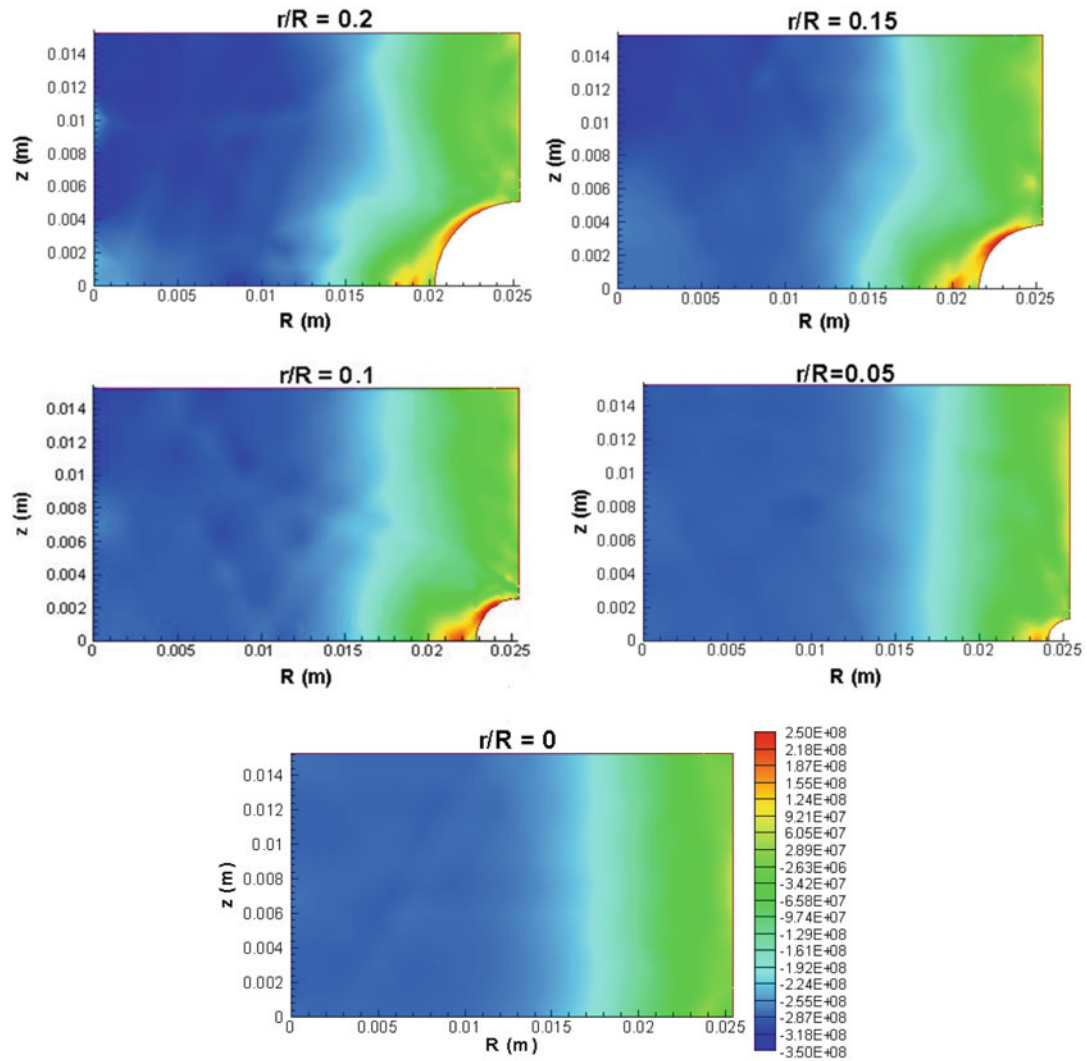


Fig. 15 Stress component σ_r distribution for different geometries

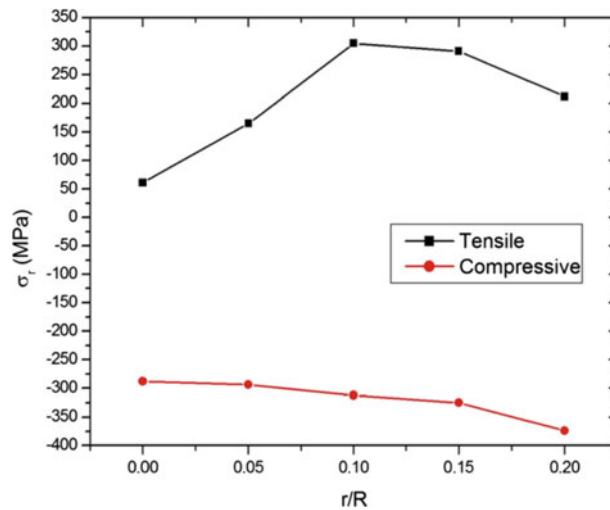


Fig. 16 Maximum σ_r stresses, tensile and compressive: comparison of mechanical behavior of pieces with stress concentrators, submitted to quenching process using water as cooling medium

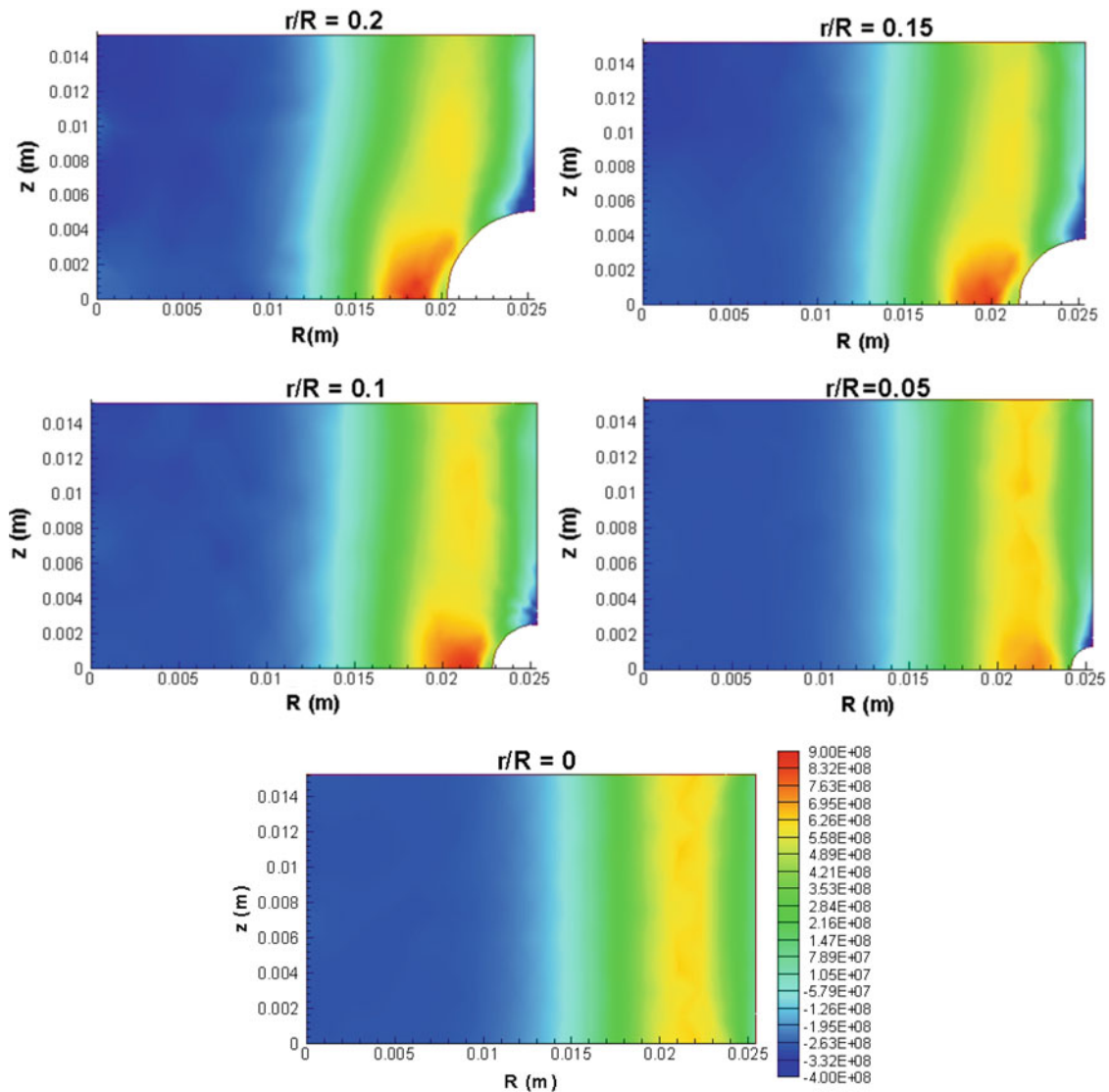


Fig. 17 Stress component σ_θ distribution for different geometries

3.3 Residual stresses

This section investigates the residual stresses that result from the quenching process. The use of water as a cooling medium makes quenching a severe process to the specimen. Under this condition, the mechanical behavior observed at the cylinder surface is more intense than other regions of the cylinder. Transformation plasticity plays an important role in this process changing the residual stress distribution. Figure 11 shows the residual stress distribution for air and water cooling media at the end of the quenching process when temperatures tend to be homogeneous in the whole piece and it is possible to identify permanent strains in the specimen. As expected, water cooling presents large values when compared with air cooling.

4 Analysis of stress concentration

This section presents an analysis of stress concentration in steel cylindrical bodies subjected to quenching. Essentially, residual stress distributions that occur during the quenching process are analyzed for different geometries. Cylindrical bodies with radius of 25.4 mm and height of 15.24 mm are treated. Stress concentration promoted by circumferential grooves with radius that varies from 0.00 to 5.08 mm is treated. Circumferential

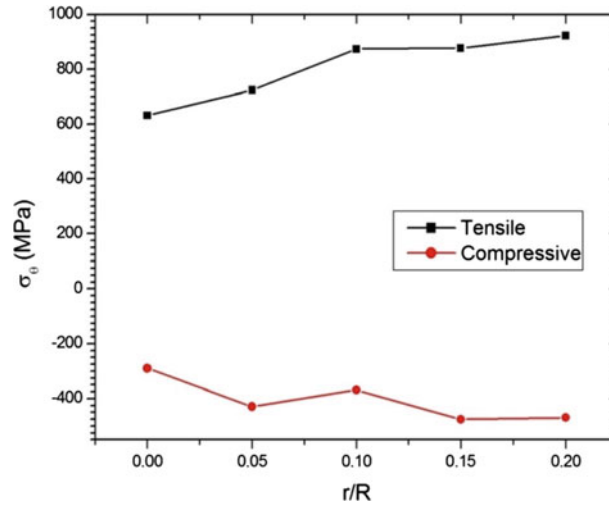


Fig. 18 Maximum σ_θ stresses, tensile and compressive: comparison of mechanical behavior of pieces with stress concentrators, submitted to quenching process using water as cooling medium

grooves are geometrical discontinuities with considerable interest in engineering since they are related to several machine elements as shafts with shoulder relief grooves or retainers grooves for spring washers.

Since water is the most severe quenching condition here investigated, it is assumed as a cooling medium. Moreover, in order to represent the behavior of a region of the cylinder subjected to progressive induction hardening [42], mechanical boundary conditions are assumed to have constrained displacements at the top and the bottom surfaces of the cylinder, as presented in Fig. 12. Different geometrical configurations are treated as shown in Fig. 13. Basically, notches with five different radius are considered assuming the following values of the ratio r/R : 0, 0.05, 0.10, 0.15, 0.20. Finite element discretization is defined by meshes chosen after a convergence analysis that took into account time and space discretization.

4.1 Final state analysis

Initially, phase transformation is investigated showing volume fraction distribution at the end of the quenching process for each one of the different geometries. Figure 14 presents the martensitic volume fraction distribution showing that the stress concentration tends to induce phase transformation. Note that martensite is the predominant phase, with minimal volume fraction of 0.81 at the center of the cylinder and maximum value of 1 at the cylinder surface.

A discussion about the residual stress distribution during the quenching process is now in focus. Basically, each one of the normal stress components (σ_r , σ_θ and σ_z) and the *von Mises* stresses are of concern. Initially, the final time instant state is treated dedicating special attention to the identification of tensile and compressive values; *von Mises* stresses are also evaluated. Afterward, spatial distribution is treated by considering the stress values in different points of the notch, for different geometries. Finally, the evolution of stress distribution through different time instants is investigated, showing the evolution of stress components during the quenching process.

Figure 15 presents the distribution of σ_r stress at the final time instant. The higher tensile stress occurs around the stress concentrator, while the higher compression values are observed in a region close to the center of the body. Figure 16 summarizes higher tensile and compressive stresses for all geometries. It should be highlighted that the higher tensile stress occurs at the piece with stress concentrator $r/R = 0.10$ and the higher compressive stress occurs at the piece with stress concentrator $r/R = 0.20$.

An analysis of σ_θ stress component is now of concern. Figure 17 presents the stress distribution at the final time instant that shows that the higher tensile stress occurs close to the stress concentrator (about 0.5 mm far), while the higher compression values are observed in a region close to the center of the cylinder. Figure 18 summarizes higher tensile and compressive stresses showing that stress concentrator $r/R = 0.20$ presents higher tensile stresses and the higher compressive stress occurs at the piece with stress concentrator $r/R = 0.15$.

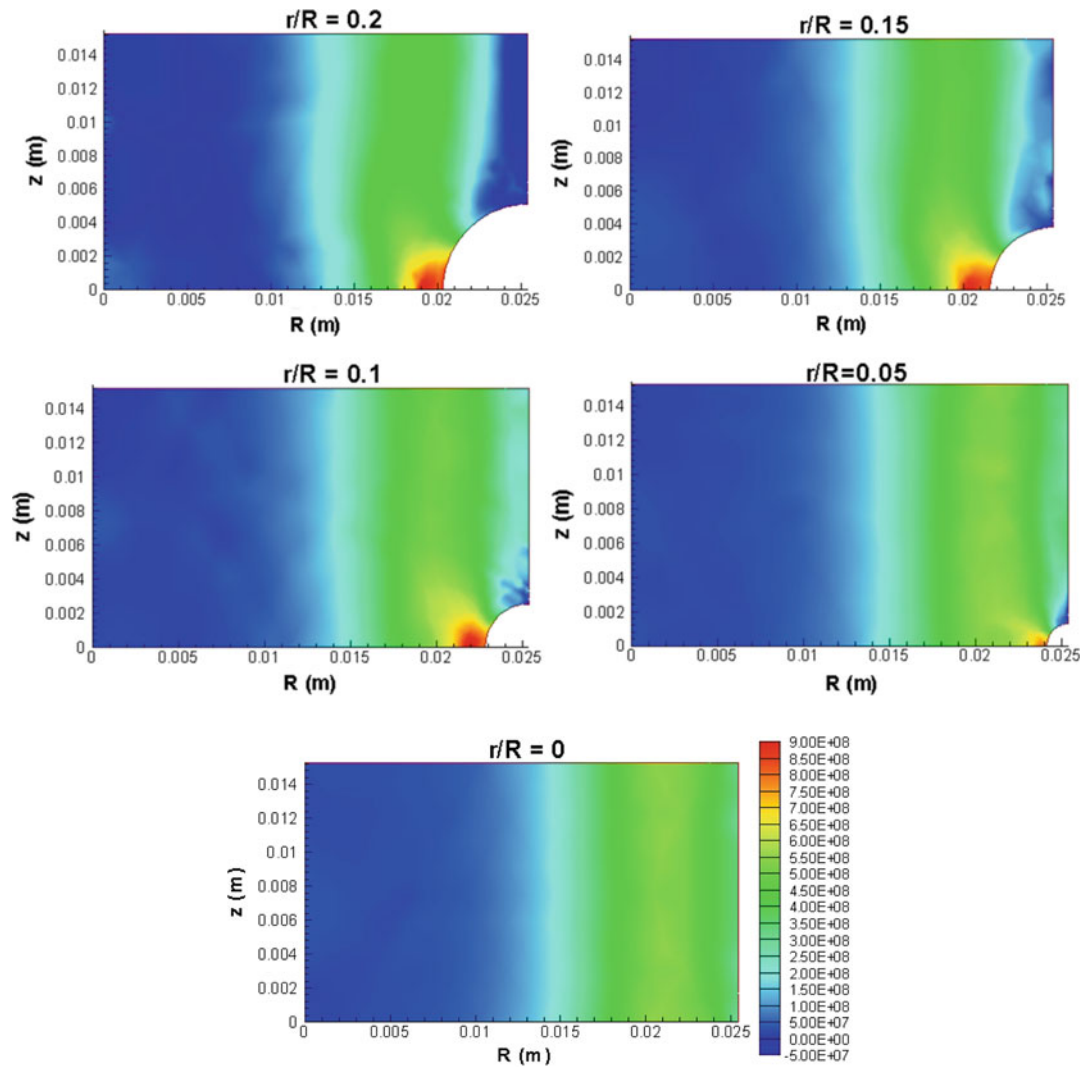


Fig. 19 Stress component σ_z distribution for different geometries

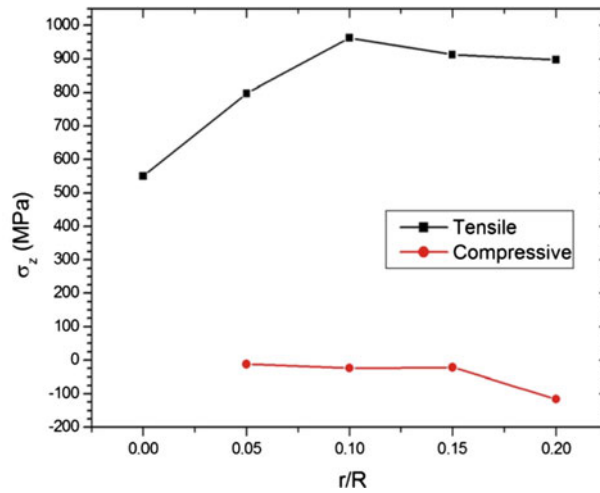


Fig. 20 Maximum σ_z stresses, tensile and compressive: comparison of mechanical behavior of pieces with stress concentrators, submitted to quenching process using water as cooling medium

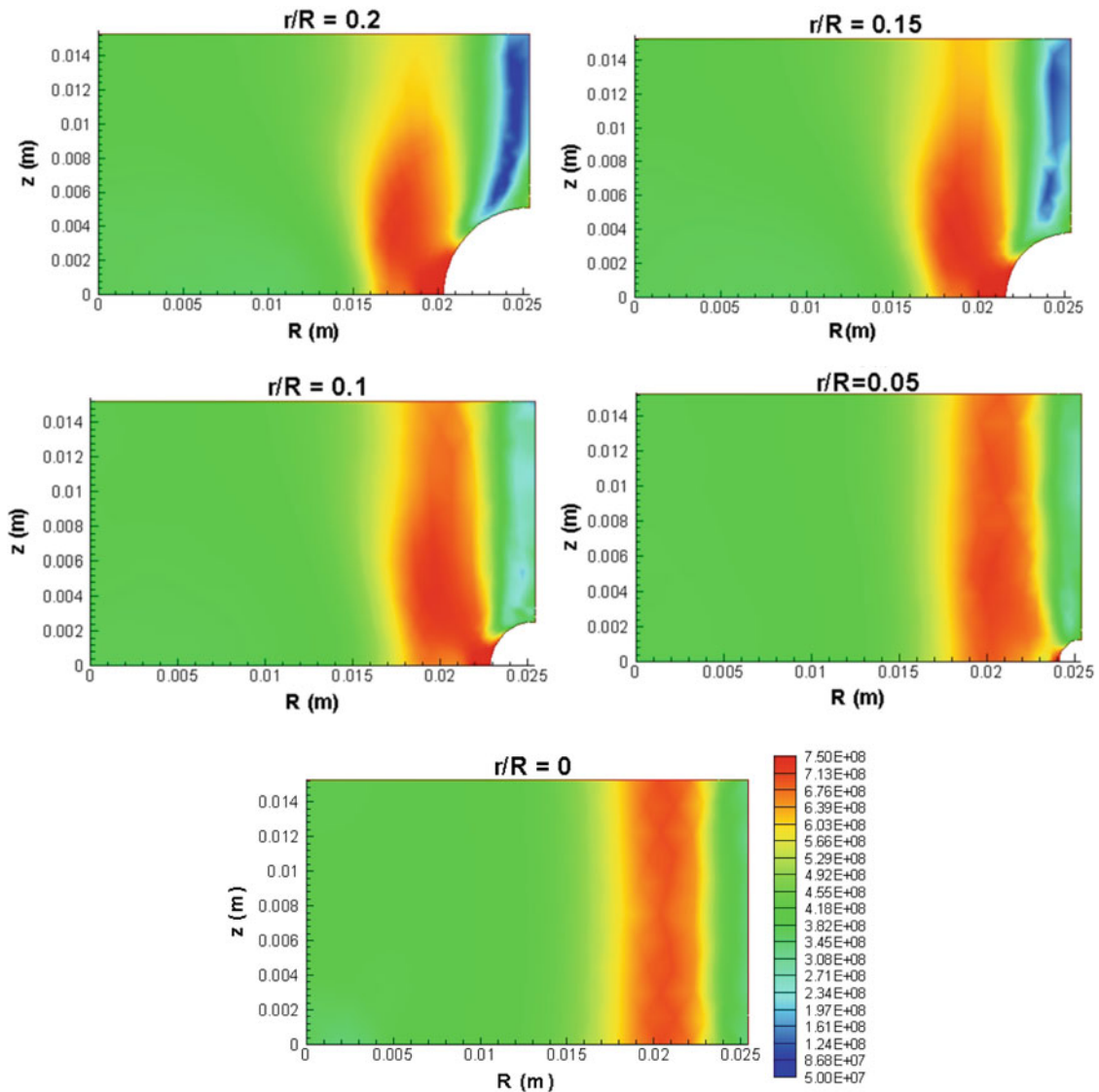


Fig. 21 von Mises stresses distribution for different geometries

Stress σ_z distribution is now focused on, as shown in Fig. 19. The higher tensile stress occurs in the deep region of the stress concentrator and the higher compression values are observed in a region close to the center of the cylinder. It is important to mention that in the piece with $r/R = 0.20$, a relevant compressive region at surface is observed. Figure 20 presents a summary of higher tensile and compressive stresses that shows that the higher tensile stress occurs at the piece with stress concentrator $r/R = 0.10$ while the higher compressive stress occurs at the piece with stress concentrator $r/R = 0.20$.

An alternative to observe the stress analysis is the von Mises stress distribution. Figure 21 presents this equivalent stress distribution for the five different geometries at the final time instant. The higher stress occurs in a region close to the stress concentrator. Figure 22 summarizes these results presenting higher stress values. The presented results show that the von Mises stress, at the high stress region, has a direct relation to stress concentrator radius, however, the difference between the higher stress of the piece with stress concentrator $r/R = 0.15$ and the higher stress of the piece without stress concentrator is equal to 64 MPa. This leads that stress concentration presents a low influence in the final residual von Mises stresses.

The stress distribution at the notch is now evaluated by considering specific points of the notch. Basically, three different points at the stress concentration region is of concern (*i*, *ii* and *iii*), as shown in Fig. 23. Figure 24 presents a comparison of stress concentrator radius sensitivity for each one of these points. Stress

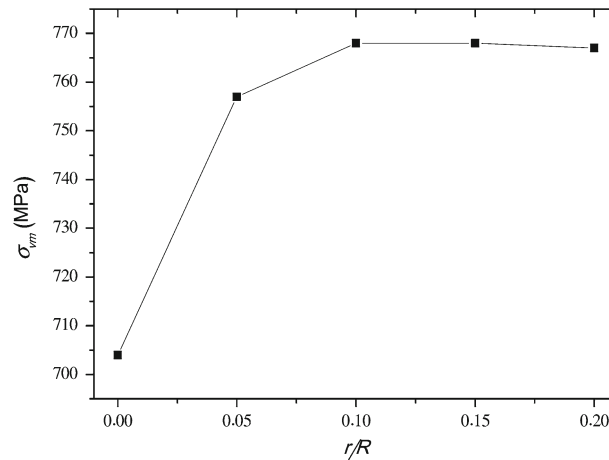


Fig. 22 Maximum $\sigma_{von Mises}$ stresses: comparison of mechanical behavior of pieces with stress concentrators, subjected to quenching process using water as cooling medium

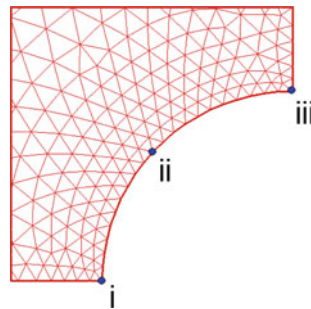


Fig. 23 Points for stress concentrator evaluation

components σ_r , σ_θ , σ_z and also the equivalent *von Mises* stress, $\sigma_{von Mises}$, are plotted against ratio r/R for each one of the three points showing the general behavior. The most sensitive stresses are σ_θ and σ_z (about 67% higher than the other stresses, in magnitude). Another observation is that σ_θ and σ_z stresses are more sensitive at the *i* and *iii* points, nevertheless, the σ_r stresses are more sensitive at the point *ii*.

4.2 Time evolution analysis

Until this moment, all results are related to the final state of cylindrical bodies subjected to quenching. This final state, however, could not be the critical one. Therefore, it is important to evaluate time evolution of stresses. The forthcoming analysis considers a geometry with stress concentrator $r/R = 0.2$ and water as cooling medium. Figures 25, 26, 27 and 28 present, respectively, the evolution of σ_r , σ_θ , σ_z and $\sigma_{von Mises}$ stresses, for different time instants during the quenching process. Basically, it is considered representative instants related to different stages of the quenching process.

The time evolution of stress components is described through steps related to the main phenomena observed: high temperature (cooling starts), phase transformation and low temperature (cooling ends). Before the cooling starts, σ_r , σ_θ and $\sigma_{von Mises}$ present very low values in the whole piece. The displacement constraint applied to the top and base of the cylinder generates σ_z stresses with values around 500 MPa in the whole piece. During the high temperature stage, phase transformations do not take place and the quick cooling at cylinder surface, due to convection phenomenon, promotes a contraction of this region, while the center of the cylinder is not experiencing this kind of behavior. All components present low variation in stress distribution.

The phase transformation stage includes transformation from austenite to different phases where martensite is the most important one. The volumetric expansion related to the phase transformations occurs with elevated temperature gradients and high cooling rates. Initially, the volumetric expansion related to martensitic transformation is the most important effect in stress distribution and, afterward, the cooling process becomes

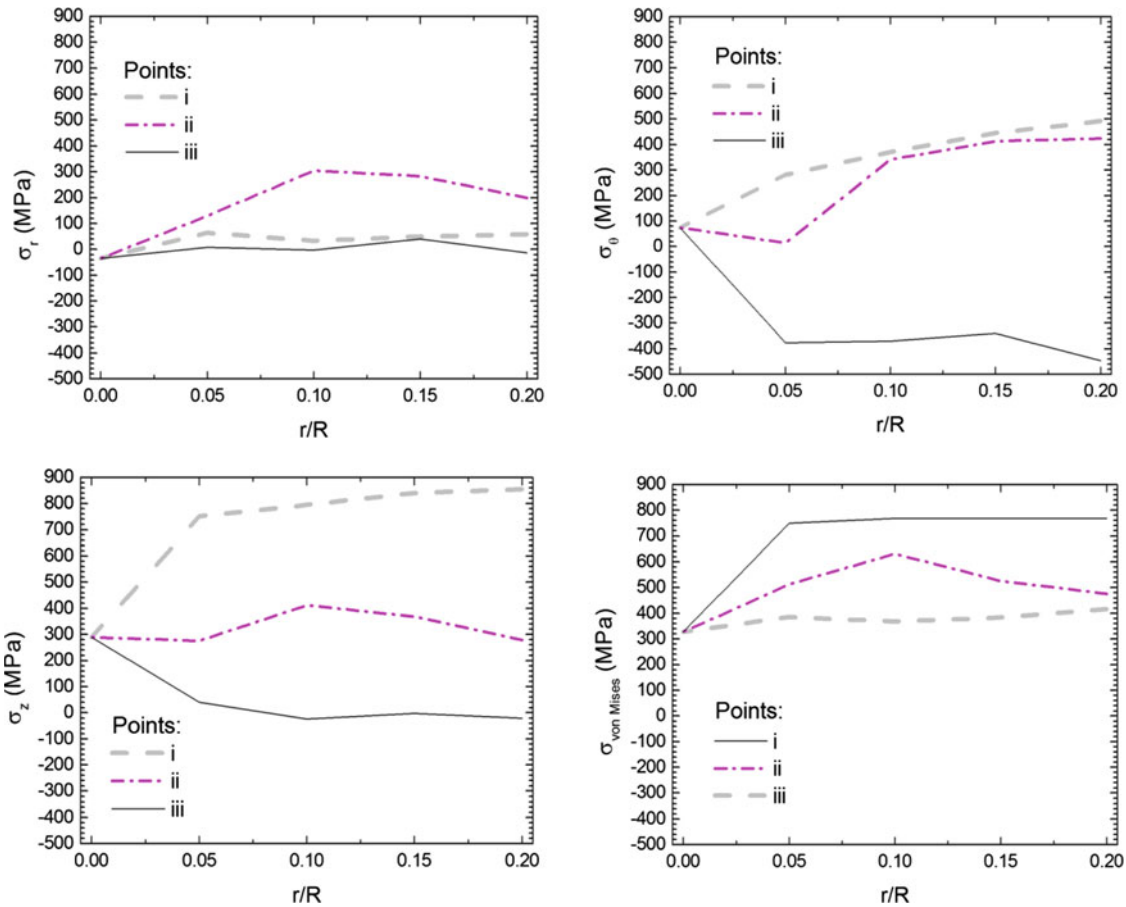


Fig. 24 Stress analysis at notch points *i*, *ii* and *iii*

preponderant. During this stage, σ_r develops compressive values at the center of the cylinder and low value tensile components at the cylinder surface; a region with tensile behavior (magnitude of 250 MPa) is developed close to the stress concentrator; σ_θ evolution initially develops compressive values at the cylinder surface, followed by compressive components close to the center of the cylinder center; at the end of the process, tensile stresses appear, with values around 900 MPa. The process can be understood as a stress increase with a seed at the most deep region of the stress concentrator; σ_z evolution initially develops a region with low stresses, located in close to the 1/3 of cylinder radius. After that, tensile stresses appear with an increase with a seed at the most deep region of the stress concentrator. Finally, this tensile region becomes a stripe from the stress concentrator to the cylinder surface, with tensile stresses that reaches values around 900 MPa. Concerning *von Mises* equivalent stress, it first develops a stress-level elevation in a region close to 1/2 of the cylinder radius; the formation of a region with elevated stress close to the cylinder surface is also observed (values around 770 MPa). Afterward, high values of stresses appear with an increase with a seed at the deep region of stress concentrator. This region grows, becoming a stripe from stress concentrator to the cylinder top, with stresses that reaches values around 770 MPa. In general, an elevation of *von Mises* stress can be observed in almost the whole piece.

The low temperature stage presents no phase transformations and the temperature becomes homogeneous through the whole piece. During this stage, all stress components present low variations.

5 Conclusions

This contribution deals with the modeling and simulation of the quenching process, presenting an anisothermal multi-phase constitutive model formulated within the framework of continuum mechanics and thermodynamics of irreversible processes. A numerical procedure is developed based on the operator split technique associated

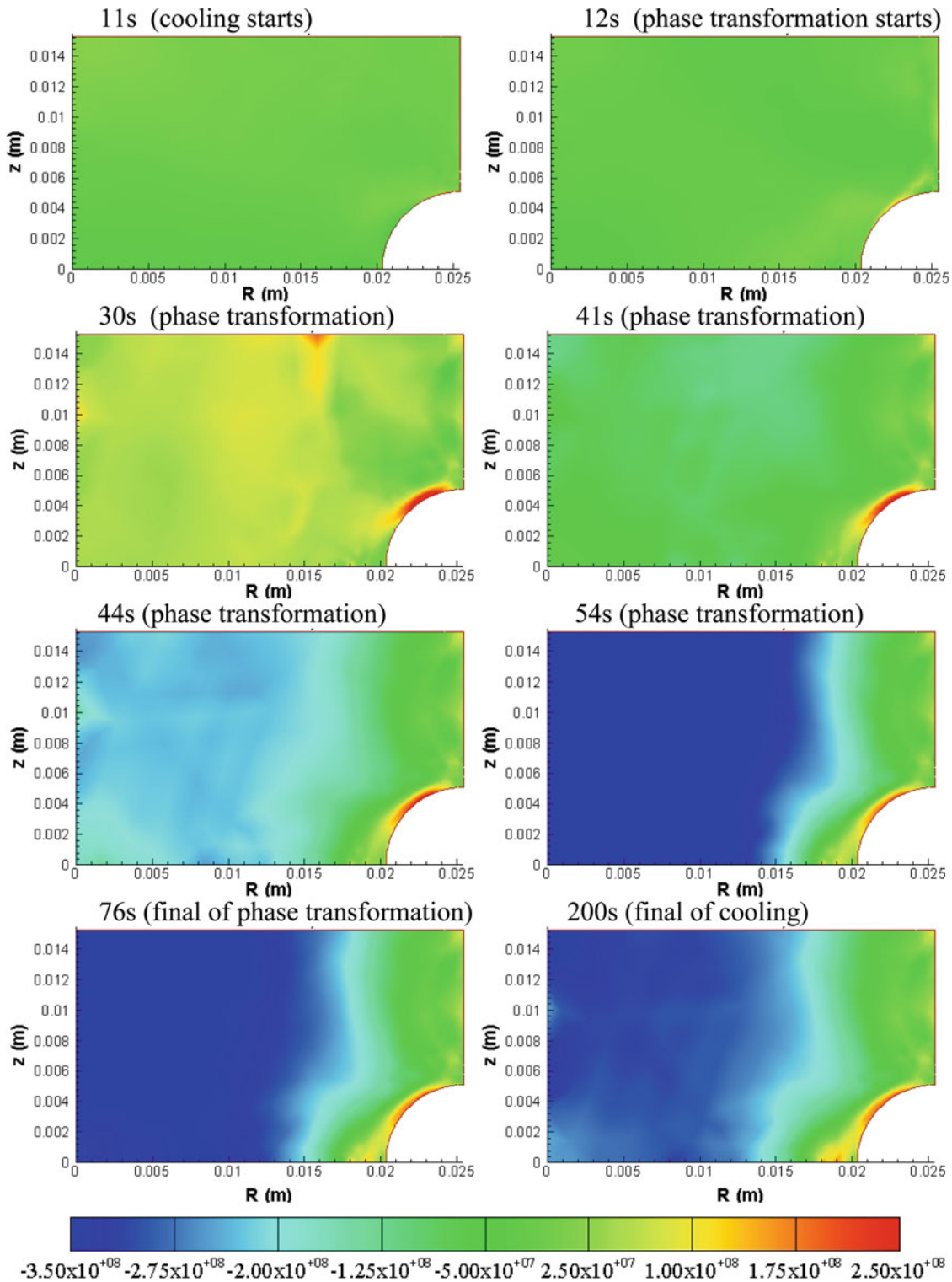


Fig. 25 Stress component σ_r distribution along the cylinder geometry for different time instants

with an iterative numerical scheme in order to deal with nonlinearities in the formulation. The finite element method is employed to perform spatial discretization together with other classical approaches. The through hardening of cylindrical bodies is considered as application of the proposed general formulation. Numerical

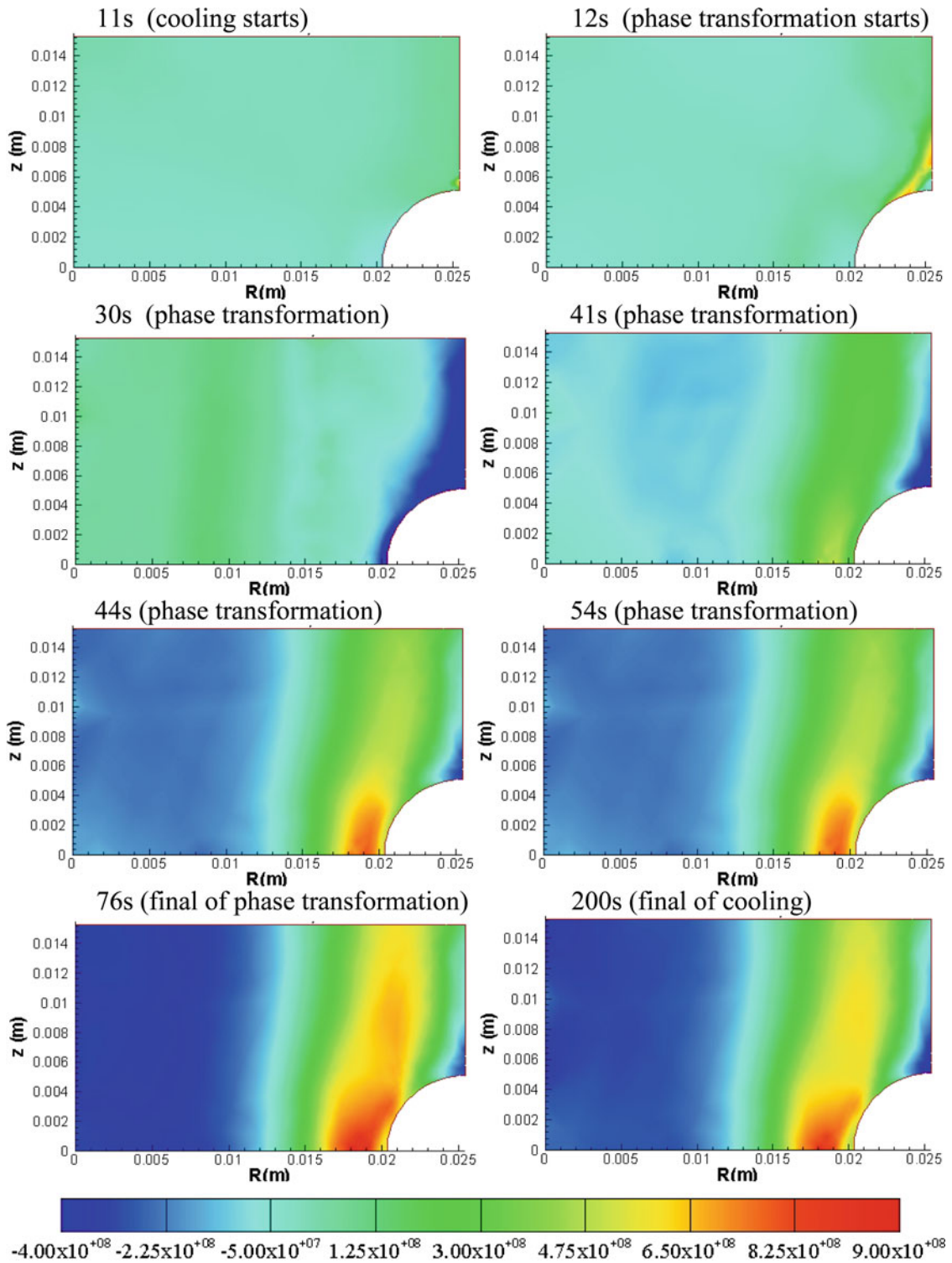


Fig. 26 Stress component σ_θ distribution along the cylinder geometry for different time instants

results establish a model verification using experimental data as a reference. Afterward, stress analysis shows the general thermomechanical behavior during the quenching process. Notched steel cylinder is also of concern evaluating the geometric influence in the thermomechanical behavior during quenching process. Phase

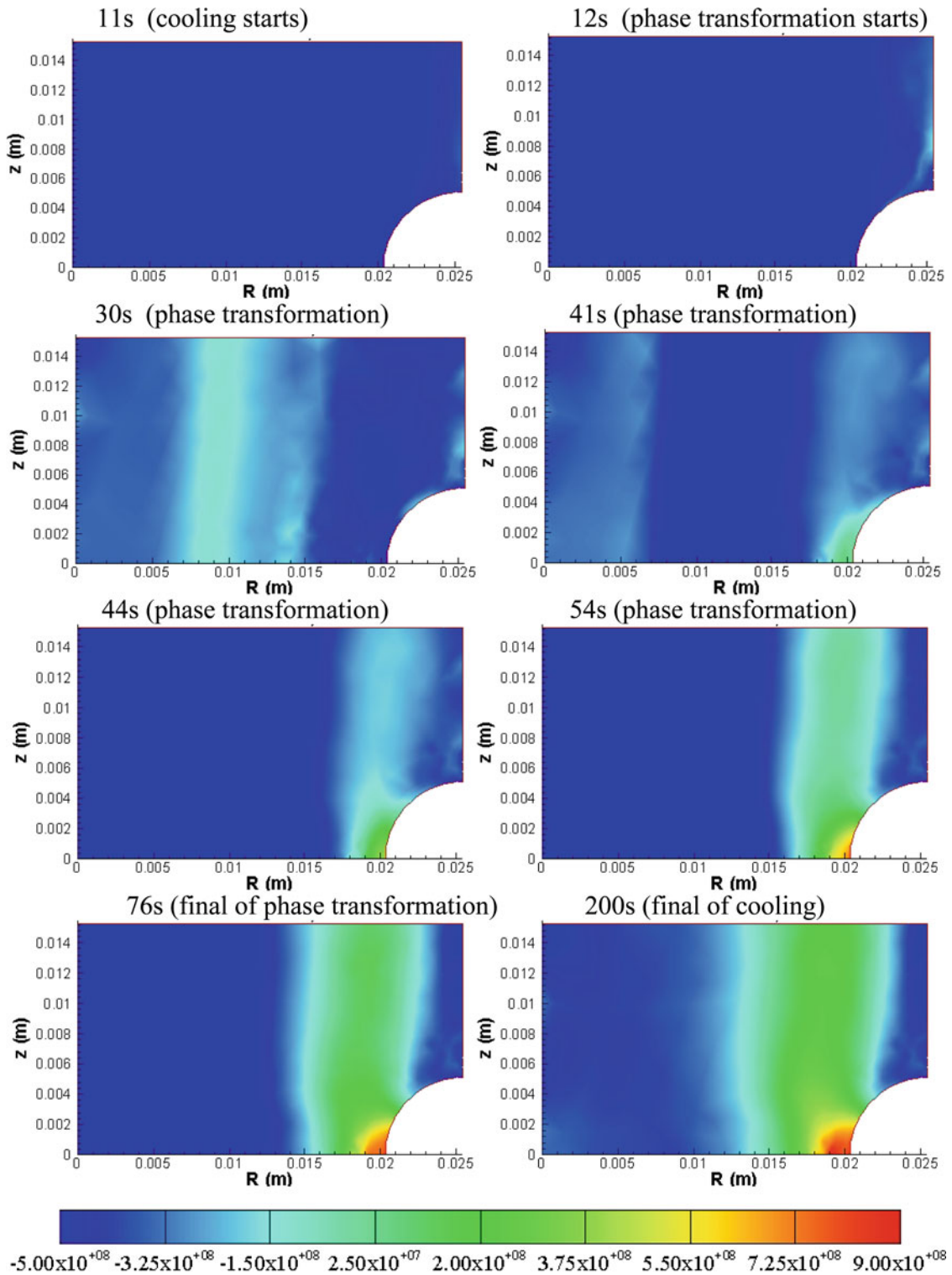


Fig. 27 Stress component σ_z distribution along the cylinder geometry for different time instants

transformations and stress analysis are carried out. Residual stress analysis considers either the final time instant state or the time evolution during the process. In general, it is possible to say that the proposed model is capable of capturing the general quenching behavior, and therefore, it can be used as a tool to predict the thermomechanical behavior of quenched mechanical components.

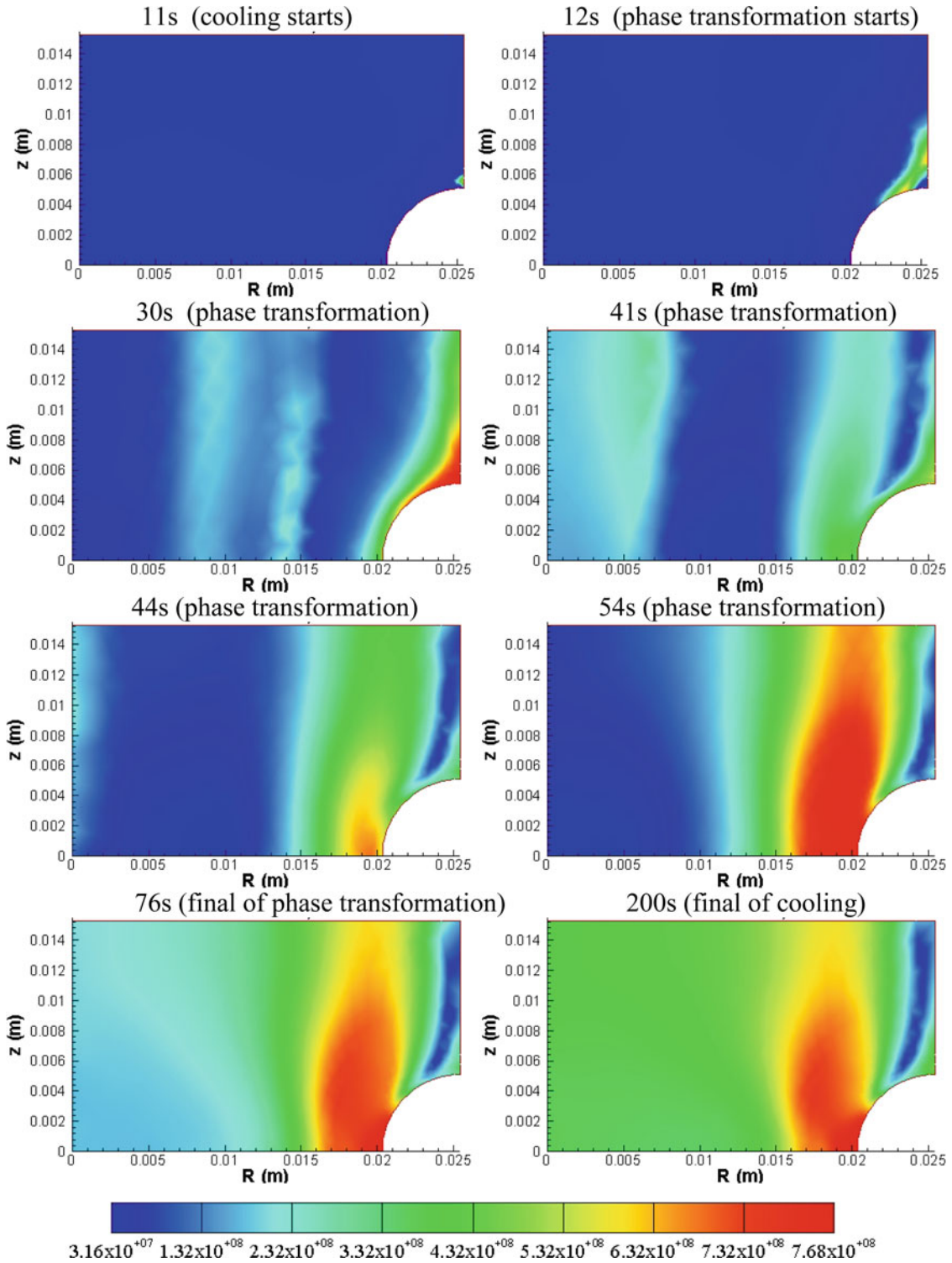


Fig. 28 von Mises stress distribution along the cylinder geometry for different time instants

Acknowledgments The authors would like to acknowledge the support of the Brazilian Research Agencies CNPq and FAPERJ and through the INCT-EIE (National Institute of Science and Technology—Smart Structures in Engineering) the CNPq and FAPEMIG. The Air Force Office of Scientific Research (AFOSR) is also acknowledged.

References

1. Avrami, M.: Kinetics of phase change. II: Transformation-time relations for random distribution of nuclei. *J. Chem. Phys.* **8**, 212 (1940)
2. Boyer, H. (ed.): Atlas of Isothermal Transformation and Cooling Transformation Diagrams. American Society for Metals (1977)
3. Cahn, J.W.: Transformation kinetics during continuous cooling. *Acta Metallurgica* **4**, 572–575 (1956)
4. Carlone, P., Palazzo, G.S., Pasquino, R.: Finite element analysis of the steel quenching process: temperature field and solid–solid phase change. *Comput. Math. Appl.* **59**(1), 585–594 (2010)
5. Çetinel, H., Toparlı, M., Özsoyeller, L.: A finite element based prediction of the microstructural evolution of steels subjected to the tempcore process. *Mech. Mater.* **32**, 339–347 (2000)
6. Chen, J.R., Tao, Y.Q., Wang, H.G.: A study on heat conduction with variable phase transformation composition during quench hardening. *J. Mater. Process. Technol.* **63**, 554–558 (1997)
7. Denis, S.: Considering stress-phase transformation interaction in the calculation of heat treatment residual stresses. *J. de Physique IV* **6**, 159–174 (1996)
8. Denis, S., Gautier, E., Simon, A., Beck, G.: Stress–phase–transformation interactions—basic principles, modelling and calculation of internal stresses. *Mater. Sci. Technol.* **1**, 805–814 (1985)
9. Denis, S., Sjöström, S., Simon, A.: Coupled temperature, stress, phase transformation calculation model numerical illustration of the internal stresses evolution during cooling of a eutectoid carbon steel cylinder. *Metall. Trans. A* **18**, 1203–1212 (1987)
10. Denis, S., Archambault, S., Aubry, C., Mey, A., Louin, J.C., Simon, A.: Modelling of phase transformation kinetics in steels and coupling with heat treatment residual stress predictions. *J. de Physique IV* **9**, 323–332 (1999)
11. Ferguson, B.L., Li, Z., Freborg, A.M.: Modeling heat treatment of steel parts. *Comput. Mater. Sci.* **34**(3), 274–281 (2005)
12. Fernandes, M.B., Denis, S., Simon, A.: Mathematical model coupling phase transformation and temperature evolution during quenching of steels. *Mater. Sci. Technol.* **1**, 838–844 (1985)
13. Gür, C.H., Tekkaya, A.E.: Numerical investigation of non-homogeneous plastic deformation in quenching process. *Mater. Sci. Eng. A* **319**(321), 164–169 (2001)
14. Hamouda, A.M.S., Sulaiman, S., Lau, C.K.: Finite element analysis on the effect of workpiece geometry on the quenching of ST50 steel. *J. Mater. Process. Technol.* **119**(1–3), 354–360 (2001)
15. Herming, C., Jiang, F., Honggang, W.: Estimation of the mechanical properties of a 42CrMo steel cylinder with phase transformation during quenching. *J. Mater. Process. Technol.* **63**, 568–572 (1997)
16. Hildenwall, B.: Prediction of the Residual Stresses Created During Quenching. Ph.D. Thesis, Linköping Univ (1979)
17. Hömberg, D.: A numerical simulation of the Jominy end-quench test. *Acta Mater.* **44**(11), 4375–4385 (1996)
18. Hossain, S., Daymond, M.R., Truman, C.E., Smith, D.J.: Prediction and measurement of residual stresses in quenched stainless-steel spheres. *Mater. Sci. Eng. A* **373**, 339–349 (2004)
19. Hossain, S., Truman, C.E., Smith, D.J., Daymond, M.R.: Application of quenching to create highly triaxial residual stresses in type 316H stainless steels. *Int. J. Mech. Sci.* **48**, 235–243 (2006)
20. Huiping, L., Guoqun, Z., Shanting, N., Chuanzhen, H.: FEM simulation of quenching process and experimental verification of simulation results. *Mater. Sci. Eng. A* **452–453**, 705–714 (2007)
21. Inoue, T., Wang, Z.: Coupling between stress, temperature, and metallic structures during processes involving phase transformations. *Mater. Sci. Technol.* **1**, 845–850 (1985)
22. Ju, D.Y., Zhang, W.M., Zhang, Y.: Modeling and experimental verification of martensitic transformation plastic behavior in carbon steel for quenching process. *Mater. Sci. Eng. A* **438–440**, 246–250 (2006)
23. Jung, M., Kang, M., Lee, Y.-K.: Finite-element simulation of quenching incorporating improved transformation kinetics in a plain medium-carbon steel. *Acta Materialia* **60**(2), 525–536 (2012)
24. Kang, S.H., Im, Y.T.: Finite element investigation of multi-phase transformation within carburized carbon steel. *J. Mater. Process. Technol.* **183**, 241–248 (2007)
25. Kang, S.H., Im, Y.T.: Thermo-elasto-plastic finite element analysis of quenching process of carbon steel. *J. Mater. Process. Technol.* **192–193**, 381–390 (2007)
26. Kang, S.H., Im, Y.T.: Three-dimensional thermo-elastic–plastic finite element modeling of quenching process of plain-carbon steel in couple with phase transformation. *Int. J. Mech. Sci.* **49**, 423–439 (2007)
27. Koistinen, D.P., Marburger, R.E.: A general equation prescribing the extent of the austenite–martensite transformation in pure iron–carbon alloys and plain carbon steels. *Acta Metallurgica* **7**, 59–60 (1959)
28. Leblond, J.B., Devaux, J., Devaux, J.C.: Mathematical modelling of transformation plasticity in steels—I: case of ideal-plastic phases. *Int. J. Plast.* **5**, 551–572 (1989)
29. Lee, S.-J., Lee, Y.-K.: Finite element simulation of quench distortion in a low-alloy steel incorporating transformation kinetics. *Acta Materialia* **56**(7), 1482–1490 (2008)
30. Lee, S.-J., Pavlina, E.J., Van Tyne, C.J.V.: Kinetics modeling of austenite decomposition for an end-quenched 1045 steel. *Mater. Sci. Eng. A* **527**(13–14), 3186–3194 (2010)
31. Lemaitre, J., Chaboche, J.L.: *Mechanics of Solid Materials*. Cambridge University Press, Cambridge (1990)
32. Li, H., Zhao, G., He, L., Mo, Y.: Solution of non-linear thermal transient problems by a new adaptive time-step method in quenching process. *Appl. Math. Model.* **33**(1), 329–342 (2009)
33. Lingamanaik, S.N., Chen, B.K.: Thermo-mechanical modelling of residual stresses induced by martensitic phase transformation and cooling during quenching of railway wheels. *J. Mater. Process. Technol.* **211**, 1547–1552 (2011)
34. Melander, M.: A Computational and Experimental Investigation of Induction and Laser Hardening, Ph.D. Thesis, Department of Mechanical Eng., Linköping University (1985)
35. Murthy, Y.V.L.N., Rao, G.V., Iyer, P.K.: Numerical simulation of welding and quenching processes using transient thermal and thermo-elasto-plastic formulations. *Comput. Struct.* **64**(1), 131–154 (1996)
36. Nallathambiah, A.K., Kaymakb, Y., Spechta, E., Bertram, A.: Sensitivity of material properties on distortion and residual stresses during metal quenching processes. *J. Mater. Process. Technol.* **210**(2), 204–211 (2010)

37. Oliveira, W.P., Savi, M.A., Pacheco, P.M.C.L., Souza, L.F.G.: Thermomechanical analysis of steel cylinders quenching using a constitutive model with diffusional and non-diffusional phase transformations. *Mech. Mater.* **42**(1), 31–43 (2010)
38. Oliveira, W.P.: Modeling and Simulation of Quenching in Axisymmetrical Geometries Using a Multi-phase Constitutive Model, Ph.D. Thesis, COPPE/UFRJ (in Portuguese) (2008)
39. Oliveira, W.P.: Modeling Quenching Process in Steel Cylinder Using Multi-phase Constitutive Model, M.Sc. Dissertation, CEFET/RJ (in Portuguese) (2004)
40. Ortiz, M., Pinsky, P.M., Taylor, R.L.: Operator split methods for the numerical solution of the elastoplastic dynamic problem. *Comput. Methods Appl. Mech. Eng.* **39**, 137–157 (1983)
41. Pacheco, P.M.C.L.: Analysis of Thermomechanical Coupling in Elasto–viscous–plastic Materials, Ph.D. Thesis, Department of Mechanical Engineering, PUC-Rio (1994)
42. Pacheco, P.M.C.L., Savi, M.A., Camarão, A.F.: Analysis of residual stresses generated by progressive induction hardening of steel cylinders. *J. Strain Anal. Eng. Des.* **36**(5), 507–516 (2001)
43. Rammerstorfer, F.G., Fischer, D.F., Mitter, W., Bathe, K.J., Snyder, M.D.: On thermo-elastic-plastic analysis of heat-treatment processes including creep and phase changes. *Comput. Struct.* **13**, 771–779 (1981)
44. Reti, T., Fried, Z., Felde, I.: Computer simulation of steel quenching process using a multi-phase transformation model. *Comput. Mater. Sci.* **22**, 261–278 (2001)
45. SAE: SAE J404-2000 chemical compositions of SAE alloy steels. *Soc. Automot. Eng.* (2000)
46. Sen, S., Aksakal, B., Ozel, A.: Transient and residual thermal stresses in quenched cylindrical bodies. *Int. J. Mech. Sci.* **42**(10), 2013–2029 (2000)
47. Silva, E.P., Pacheco, P.M.C.L., Savi, M.A.: On the thermo-mechanical coupling in austenite–martensite phase transformation related to the quenching process. *Int. J. Solids Struct.* **41**(3–4), 1139–1155 (2004)
48. Silva, E.P., Pacheco, P.M.C.L., Savi, M.A.: Finite element analysis of the phase transformation effect in residual stresses generated by quenching in notched steel cylinders. *J. Strain Anal. Eng. Des.* **40**(2), 151–160 (2005)
49. Silva, E.P.: Modeling and Simulation of Steel Quenching Process Using Finite Element Method. M.Sc. Dissertation, Department of Mechanical and Materials Engineering, Instituto Militar de Engenharia (in Portuguese) (2002)
50. Şimşir, C. & Gür, C.H.: 3D FEM simulation of steel quenching and investigation of the effect of asymmetric geometry on residual stress distribution. *J. Mater. Process. Technol.* **207**(1–3), 211–221 (2008)
51. Şimşir, C., Gür, C.H.: A simulation of the quenching process for predicting temperature, microstructure and residual stresses. *J. Mech. Eng.* **56**(2), 93–103 (2010)
52. Simo, J.C., Hughes, T.J.R.: *Computational Inelasticity*. Springer, Berlin (1998)
53. Sinha, V.K., Prasad, R.S., Mandal, A., Maity, J.: A mathematical model to predict microstructure of heat-treated steel. *J. Mater. Eng. Perform.* **16**(4), 461–469 (2007)
54. Sjöström, S.: Interactions and constitutive models for calculating quench stresses in steel. *Mater. Sci. Technol.* **1**, 823–829 (1985)
55. Stull, D.R., Prophet, H.: *Janaf Thermochemical Tables*. National Standard Ref. Data System, 2 Ed. NBS 37 (1971)
56. Ulysse, P.: Thermo-mechanical characterization of forged coated products during water quench. *J. Mater. Process. Technol.* **209**(15–16), 5584–5592 (2009)
57. Wang, K.F., Chandrasekar, S., Yang, H.T.Y.: Finite-element simulation of moving induction heat treatment. *J. Mater. Eng. Perform.* **4**(4), 460–473 (1995)
58. Woodard, P.R., Chandrasekar, S., Yang, H.T.Y.: Analysis of temperature and microstructure in the quenching of steel cylinders. *Metall. Mater. Trans. B* **30**(4), 815–822 (1999)